Resource

Cell Metabolism

Extracellular Vesicles Provide a Means for Tissue Crosstalk during Exercise

Graphical Abstract

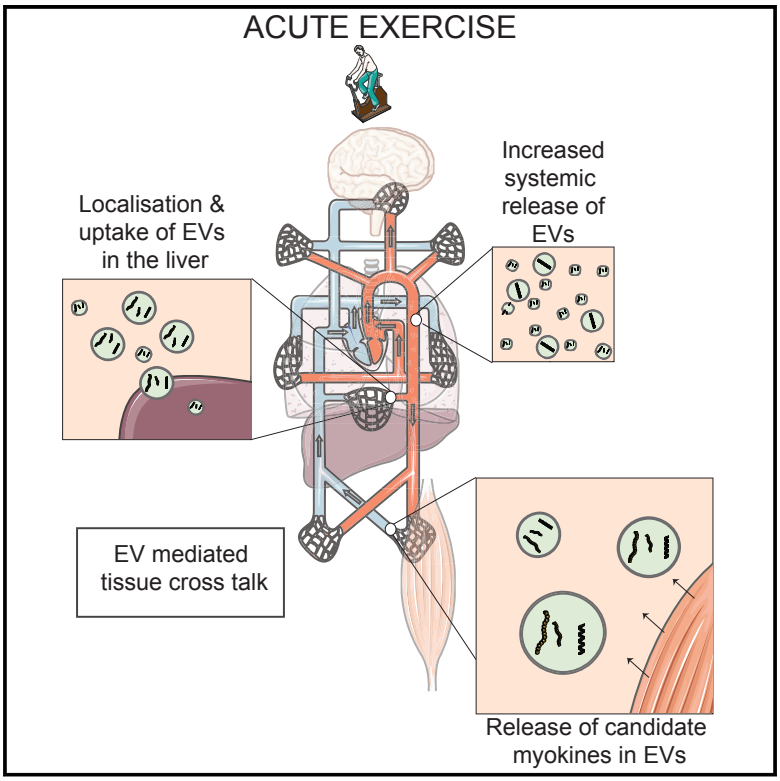

Authors

Martin Whitham, Benjamin L. Parker, Martin Friedrichsen, ..., David E. James, Jørgen F.P. Wojtaszewski, Mark A. Febbraio

Correspondence

martwhitham@gmail.com (M.W.), m.febbraio@garvan.org.au (M.A.F.)

In Brief

Using quantitative proteomic techniques and intravital imaging experiments, Whitham et al. characterize the exercise-induced secretion of proteins contained in extracellular vesicles (EVs) and identify several novel candidate myokines that are released into the circulation independently of classical secretion.

Highlights

- Exosomes and small vesicles are released into circulation with exercise
- Proteins without a signal peptide sequence circulate in vesicles during exercise
- Exercise-liberated vesicles have a propensity to localize in the liver
- Femoral arteriovenous difference analysis identifies 35 novel candidate myokines

Whitham et al., 2018, Cell Metabolism *27*, 237–251
January 9, 2018 © 2017 Elsevier Inc.
https://doi.org/10.1016/j.cmet.2017.12.001

CellPress

Cell Metabolism
Resource

Extracellular Vesicles Provide a Means for Tissue Crosstalk during Exercise

Martin Whitham,[1,7,*] Benjamin L. Parker,[2] Martin Friedrichsen,[3] Janne R. Hingst,[3] Marit Hjorth,[1,7] William E. Hughes,[1,7] Casey L. Egan,[1] Lena Cron,[1] Kevin I. Watt,[8] Rhiannon P. Kuchel,[4] Navind Jayasooriah,[5,6] Emma Estevez,[1] Tim Petzold,[1] Catherine M. Suter,[5] Paul Gregorevic,[8,9,10,11] Bente Kiens,[3] Erik A. Richter,[3] David E. James,[2] Jørgen F.P. Wojtaszewski,[3] and Mark A. Febbraio[1,7,12,*]

[1]Cellular and Molecular Metabolism, Garvan Institute of Medical Research, Sydney, NSW, Australia
[2]Charles Perkins Centre, School of Life and Environmental Sciences, University of Sydney, Sydney, NSW, Australia
[3]Department of Nutrition, Exercise and Sports, Faculty of Science, University of Copenhagen, Copenhagen, Denmark
[4]Electron Microscope Unit, University of New South Wales, Sydney, NSW, Australia
[5]Epigenetics Laboratory, Victor Chang Cardiac Research Institute, Sydney, NSW, Australia
[6]School of Biotechnology and Biomolecular Sciences, University of New South Wales, Sydney, NSW, Australia
[7]St Vincent's Clinical School, University of New South Wales, Sydney, NSW, Australia
[8]Baker Heart and Diabetes Institute, Melbourne, VIC, Australia
[9]Department of Physiology, University of Melbourne, Melbourne, VIC, Australia
[10]Department of Biochemistry and Molecular Biology, Monash University, Melbourne, VIC, Australia
[11]Department of Neurology, University of Washington School of Medicine, Seattle, WA, USA
[12]Lead Contact
*Correspondence: martwhitham@gmail.com (M.W.), m.febbraio@garvan.org.au (M.A.F.)
https://doi.org/10.1016/j.cmet.2017.12.001

SUMMARY

Exercise stimulates the release of molecules into the circulation, supporting the concept that inter-tissue signaling proteins are important mediators of adaptations to exercise. Recognizing that many circulating proteins are packaged in extracellular vesicles (EVs), we employed quantitative proteomic techniques to characterize the exercise-induced secretion of EV-contained proteins. Following a 1-hr bout of cycling exercise in healthy humans, we observed an increase in the circulation of over 300 proteins, with a notable enrichment of several classes of proteins that compose exosomes and small vesicles. Pulse-chase and intravital imaging experiments suggested EVs liberated by exercise have a propensity to localize in the liver and can transfer their protein cargo. Moreover, by employing arteriovenous balance studies across the contracting human limb, we identified several novel candidate myokines, released into circulation independently of classical secretion. These data identify a new paradigm by which tissue crosstalk during exercise can exert systemic biological effects.

INTRODUCTION

It is well known that exercise capacity is a powerful predictor of mortality (Korpelainen et al., 2016; Myers et al., 2002), and even short periods of physical inactivity are associated with impaired metabolic homeostasis, manifested as decreased insulin sensitivity, reduced postprandial lipid clearance, loss of muscle mass, and accumulation of visceral adiposity (Pedersen and Febbraio, 2012). These acute changes provide a link between physical inactivity and increased risk of acquiring chronic diseases such as obesity, type 2 diabetes, cardiovascular disease, and cancer (Booth et al., 2012; Febbraio, 2017; Pedersen and Febbraio, 2012). Many of the benefits of physical activity have been attributed to several mechanisms, including reduced adiposity and increased cardio-respiratory capacity, as discussed previously (Febbraio, 2017). Despite the fact that tissue crosstalk was proposed as a mechanism for the physiological effects of exercise over 60 years ago (Goldstein, 1961; Kao and Ray, 1954), the concept has been, until recently, both understudied and underappreciated. Since the turn of the millennium, however, numerous tissues such as skeletal muscle (Febbraio et al., 2004; Moon et al., 2016; Rao et al., 2014), liver (Hansen et al., 2011, 2015), adipose tissue (Hondares et al., 2011; Stanford et al., 2013), brain (Lancaster et al., 2004), and bone (Mera et al., 2016) have been shown to secrete proteins during exercise, perhaps mediating some of the benefits of physical activity and exposing the possibility for therapeutic manipulation of the positive benefits of exercise. It is important to note that most, if not all, of the previously identified proteins described above have been discovered via serendipity or transcriptomic screens that filter for gene products that possess a signal sequence peptide. As a consequence, the concept of tissue crosstalk during exercise has focused upon uncovering novel proteins or peptides, classically secreted, that act in ligand-receptor-binding complexes (for review, see Whitham and Febbraio, 2016).

Insight into the dynamic interchange of proteins between tissues via the circulation requires an approach that overcomes considerable technical hurdles. Much like the challenges facing plasma biomarker discovery (Geyer et al., 2017), identifying specific proteins in the midst of the vast proteomic complexity of plasma is not trivial (Whitham and Febbraio, 2016). Mass

spectrometry (MS)-based proteomics offers unbiased and hypothesis-free analysis of vast numbers of different proteins, sometimes exceeding as many as 10,000 in cell lines or tissue samples simplified by extensive fractionation (Mann et al., 2013). However, proteomic coverage in plasma samples has so far largely been limited to a few hundred proteins, hampered severely by the presence of highly abundant proteins such as albumin, which constitutes roughly 50% of total protein mass (Geyer et al., 2017). Without addressing this issue, therefore, only highly abundant plasma proteins are identified while proteins conceivably participating in tissue crosstalk may remain undetected.

The secretion of extracellular vesicles (EVs) from cells or tissues into the extracellular environment is an evolutionary conserved process increasingly appreciated as an essential mechanism of intercellular communication (Raposo and Stoorvogel, 2013). Healthy cells shed microvesicles of varying size from their plasma membranes. In addition, exosomes are generated within multi-vesicular endosomal compartments, which fuse with the cell membrane to be released into the extracellular environment (Kowal et al., 2014). While first assumed to contain debris with no biological significance, EVs are now recognized not only as important carriers of proteins, lipids, and nucleic acids in plasma, but also as being capable of transferring such cargo to recipient cells (Kowal et al., 2014; Raposo and Stoorvogel, 2013; Wiklander et al., 2015). Indeed, adipose tissue secretes exosomes containing microRNAs capable of regulating gene expression in the liver and other tissues (Thomou et al., 2017). Importantly, exosomes transplanted from adipose tissue macrophages of obese mice into lean mice induce an insulin-resistant phenotype, while the reverse experiment (transplantation from lean to obese mice) induces insulin sensitivity (Ying et al., 2017). Extracellular vesicle trafficking, therefore, represents an important biological process, capable of profound metabolic effects, which has been understudied in the context of tissue crosstalk during exercise. Furthermore, by focusing specifically on the EV fraction of plasma, one derives a convenient separation of lowly abundant proteins from plasma proteins such as albumin that hamper proteomic coverage. Proteomic analysis of EVs therefore facilitates an in-depth insight into protein dynamics in plasma during a complex metabolic stimulus such as exercise.

Inspired by the growing body of data implicating EVs in the participation of tissue communication, we hypothesized that exercise might stimulate EV secretion and provide a mechanism by which tissues can transfer important signaling molecules from one tissue to another. While this concept has been speculated upon in the literature (Egan et al., 2016; Frühbeis et al., 2015; Guescini et al., 2015; Safdar et al., 2016; Whitham and Febbraio, 2016; Zierath and Wallberg-Henriksson, 2015), experimental data are lacking. Here we report a temporal analysis of the exercise-induced EV proteome in human plasma taken before and after exercise. We demonstrate a robust exercise-induced increase in several classes of proteins associated with small vesicles and exosomes. We identify some of the proteomic cargo enclosed within these vesicles, demonstrate that this cargo can be transferred to recipient tissues and cells, and highlight the considerable scope with which EV trafficking can mediate biological change during exercise.

RESULTS

Deep Proteomic Analysis of EV-Cargoed Proteins via Nano-UHPLC Tandem Mass Spectrometry

EVs are present within diverse body fluids, including breast milk, saliva, and plasma, and can be isolated via a range of centrifugation, immunoaffinity, and gel filtration techniques (Pocsfalvi et al., 2016). Arguably the most typical of these methods is ultracentrifugation, with the consensus that samples require prolonged (>1 hr) centrifugation at 100,000 × *g* to isolate small vesicles and exosomes that participate in intercellular communication. However, recent progress in proteomic analyses of EV lysates has been rapid, uncovering an unappreciated depth of analytic coverage in samples derived via relatively simple high-speed centrifugation in a bench-top microcentrifuge (Harel et al., 2015). We therefore considered whether nano-ultra-high-performance liquid chromatography (UHPLC) tandem mass spectrometry (MS/MS) analysis facilitates a quantitative analysis of small EVs and exosomes in plasma when the vesicles are derived via centrifugation at 20,000 × *g*. Interestingly, we identified a host of small-vesicle and exosomal markers, including SDCBP, TSG101, PDCD6IP (ALIX), CD63, and CD9, in 20,000 × *g*-derived EV lysates of three healthy human donors (Figure S1). Further, we observed no significant quantitative differences in any EV markers between samples subjected to 20,000 or 100,000 × *g* centrifugation (Figures S1B and S1C). These data indicate that a quantitative proteomic analysis of small-vesicle and exosomal protein cargo is possible with the relative practical convenience of 2 × 60-min spins in a bench-top microcentrifuge. We show here how this analysis can reveal novel insights into dynamic changes in circulating proteins *in vivo*.

We next applied this methodology to identify the exercise-induced EV proteome. We initially analyzed plasma in samples obtained from an indwelling cannula in the femoral artery before (rest), immediately after (exercise), and 4 hr after (recovery) a 60-min bout of cycle ergometer exercise in 11 healthy males. All samples were processed for the isolation of EVs as outlined in Figure 1A. This isolation methodology gave rise to the fractionation of vesicles in the region of 50–350 nm in size, as indicated by nanoparticle tracking analysis (Figure 1B) and cryoelectron microscopy (Figure 1C). EV pellets were then analyzed by nano-UHPLC-MS/MS and identified proteins were quantified by label-free quantitation (Cox et al., 2014). In parallel, we also analyzed pooled EV lysates from the samples taken at rest and exercise fractionated via a BEH C18 HPLC column in order to create a reference proteome with which to increase protein identification in our experimental samples via feature matching (Figure 1A). In total, we detected 5,359 proteins at a false discovery rate of 1% with an expected large majority of these proteins being identified in the reference proteome (Figure 2). In agreement with recent, similar analyses of plasma-derived EVs (Harel et al., 2015; Hurwitz et al., 2016), the present dataset achieves a similar depth of proteomic coverage to the peptide atlas compendium of over 120 studies and adds ~2,780 proteins not specifically annotated as plasma proteins (Figure 2A). Furthermore, we observed a large overlap between our dataset and the manually curated EV database, Vesiclepedia (Kalra et al., 2012) (Figure 2B) and we were again able to detect a host of known exosomal and small-vesicle markers such as TSG101, CD63, CD81, CD9,

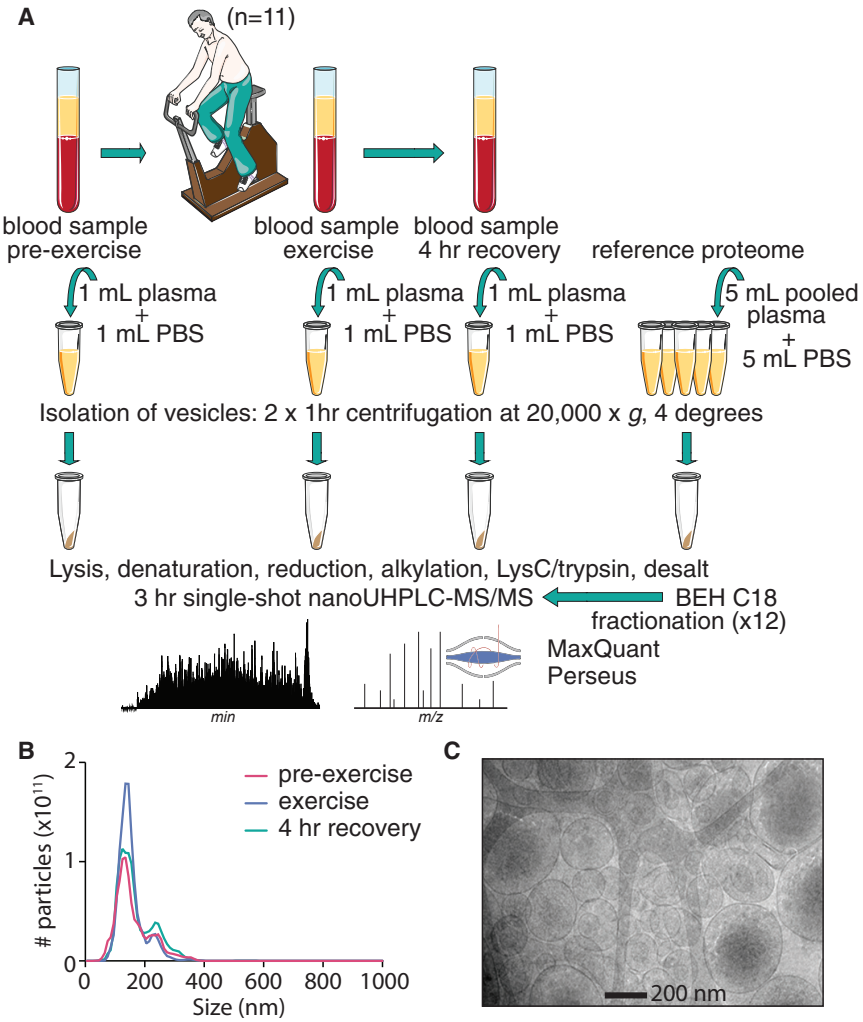

Figure 1. Methodological Approach to the Quantitative Proteomic Analysis of Exercise-Induced EV Proteins

EV pellets from plasma samples were derived from 11 healthy male participants carrying out 1 hr (30 min at 55%, 20 min at 70%, and ~10 min [until exhaustion] at 80% of VO_2max) of cycle exercise by high-speed centrifugation and subjected to nano-UHPLC-MS/MS.

(A) Both arterial and venous circulations were sampled.

(B and C) The EV isolation method gave rise to vesicles in the range of 50–350 nm in size, as indicated by nanoparticle tracking analysis (B) and visualized by cryoelectron microscopy (C).

SDCBP, EHD1, and PDCD6IP (ALIX) (Figure 2D). Strikingly, analysis of the amino acid sequences of all identified proteins via the SignalP server (Petersen et al., 2011) revealed just 16.3% had a predicted signal peptide (Figure 2C). Taken together, this implies that our optimized method targets EVs and allows in-depth analysis of the protein cargo within these vesicles, a large proportion of which are not known to be released into the circulation or to contain a signal peptide sequence.

Exercise Leads to an Increase in Circulating Small Vesicles and Exosomes

We derived a quantitative comparison of 1,199 proteins between samples taken at rest, immediately after exercise, and after 4 hr of recovery. To our knowledge, this is the first acute, temporal, *in vivo* analysis of the human plasma EV proteome. We identified 322 proteins that were significantly different between exercise and rest (Figure 2E; full list of proteins in Table S1). Furthermore, just three proteins were significantly different between rest and recovery samples, demonstrating transient effects of exercise on EV protein abundance in circulation (Figure 2E; list of proteins in Table S1). Notably, a large proportion of the upregulated proteins with exercise belong to protein groups thought to constitute small vesicles and exosomes (Figure 3A). Indeed, we observed a significant increase in proteins previously associated with multi-vesicular body formation (ALIX), membrane trafficking (Rab proteins and Annexins), chaperone (heat shock proteins) and cytoskeletal (tubulins, actins, and myosins) functions, lipid rafts (Flotilin 1 and 2), and vesicle adhesion (Integrins and tetraspanins) and signaling (14-3-3 and G proteins) (Figure 3A). By way of support for these data, nanoparticle tracking analysis of a subset of samples revealed an increase in particles in the size range attributed to small vesicles, post-exercise (Figure 1B). Further, in recognition that many previously labeled exosome markers are, in fact, not unique to small 40–150 nm vesicles and endosome-derived exosomes (Haraszti et al., 2016; Keerthikumar et al., 2015b; Kowal et al., 2016; Minciacchi et al., 2015; Willms et al., 2016), we specifically searched our data for markers previously highly enriched in small EVs. We observed a significant increase in the circulation of ACTN4 (Willms et al., 2016), ADAM10 (Kowal et al., 2016), ALIX (Haraszti et al., 2016), ANAX11 (Kowal et al., 2016), and CD81 (Haraszti et al., 2016; Keerthikumar et al., 2015b; Kowal et al., 2016). In addition, when carrying out gene ontology (GO) enrichment analysis on proteins significantly upregulated with exercise, we observed a significant enrichment of proteins associated with a variety of intracellular origins, including endosomal compartments, filopodium, and cilium (Figure 3B). Taken together, these data provide evidence that exercise leads to a significant, transient release of EVs into circulation, largely characteristic of exosomes and other small vesicles of cellular origins such as plasma membrane-derived extensions.

Exercise Induces a Release of EV-Packaged Proteins Involved in a Broad Array of Biological Processes

A significant release of small vesicles into the circulation implies that cells might communicate during exercise by packaging signaling proteins into EVs. To investigate this in greater depth, we carried out further enrichment analysis on the dataset,

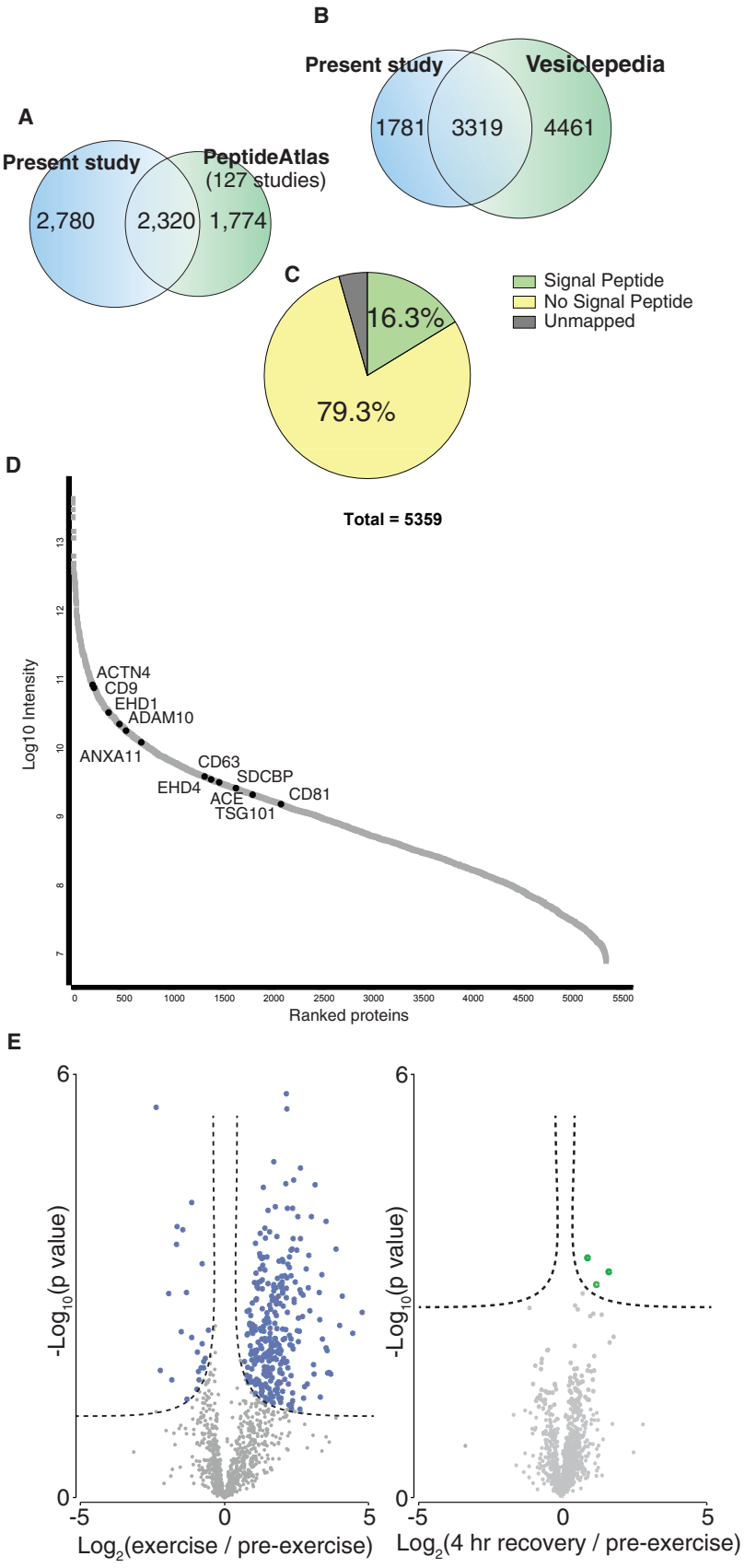

Figure 2. Deep Proteomic Coverage of the EV Proteome

(A) Venn diagram to show respective proteomic coverage in the present dataset versus the plasma section of the PeptideAtlas database. Gene products were matched in FunRich.

(B) Comparison of proteomic coverage in present data versus manually curated vesicle database Vesiclepedia.

(C) Amino acid sequences of all proteins identified were analyzed via the SignalP server to predict the presence or absence of a signal peptide sequence.

(D) Total proteomic coverage of 5,359 proteins expressed as rank versus log10 intensity. Some known small-vesicle and exosomal markers are indicated.

(E) Volcano plots depicting significant changes in proteins (isolated from EV lysates comparing exercise and rest [left] and recovery and rest [right]).

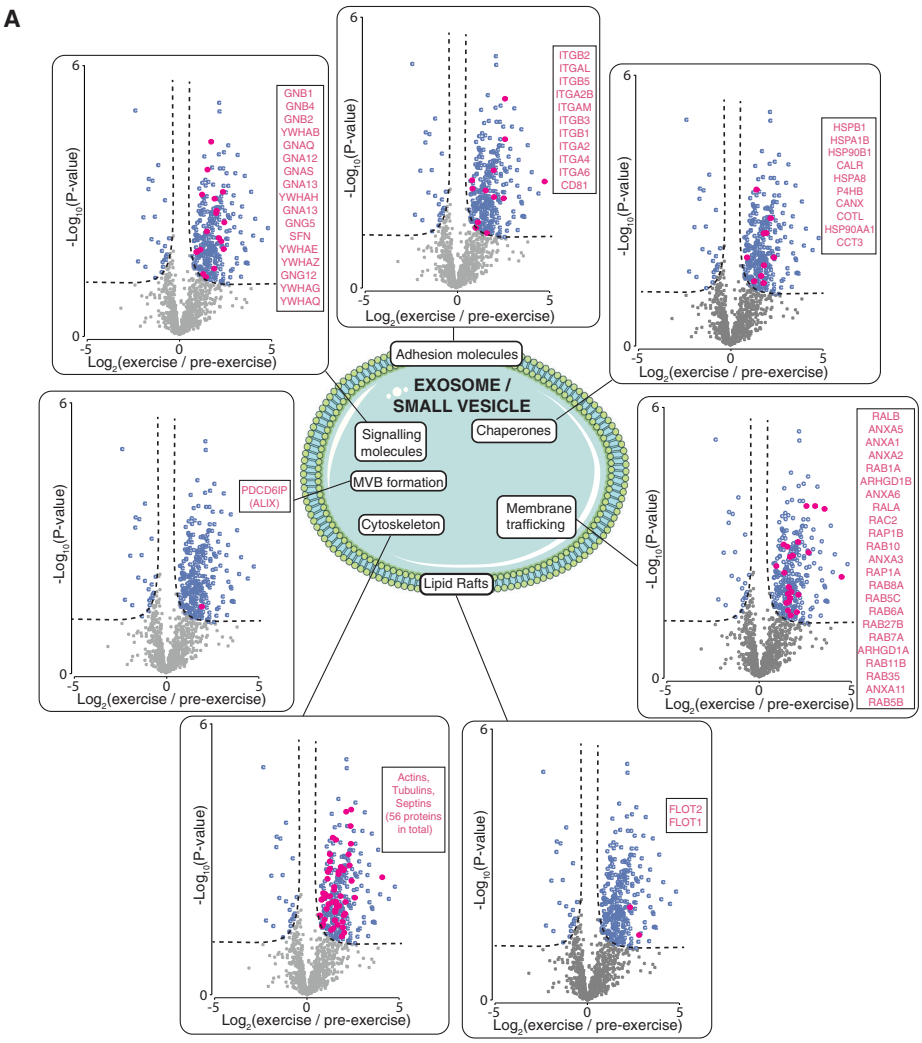

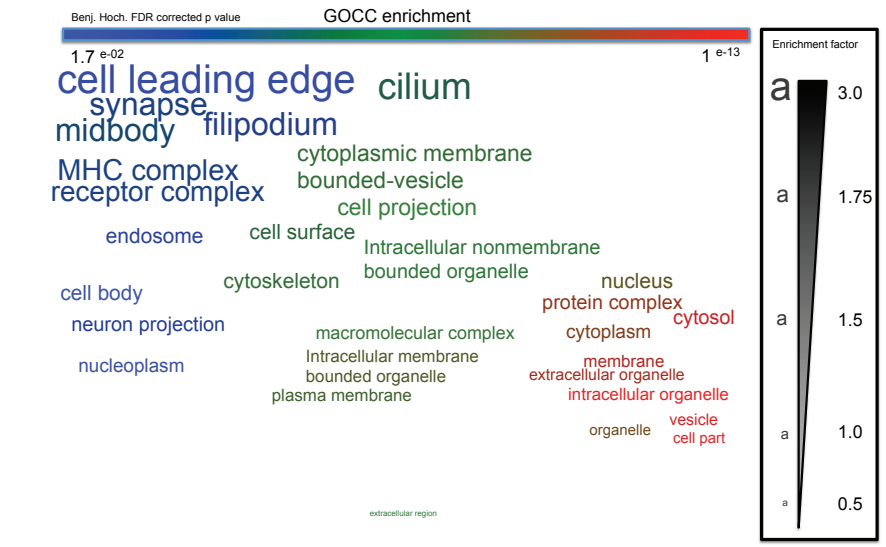

(legend on next page)

seeking non-random associations between significantly upregulated proteins and GO categorical annotations over-represented in these data, such as molecular functions and biological processes. Overall, we observed significant enrichment in 146 GO-term-defined biological processes (Figure S2A; $q < 0.02$), ranging from signal transduction to regulation of immune cell proliferation. In line with these findings, the exercise data demonstrated significant enrichments in several molecular functions, most notably G-protein and GTPase signaling (Figure S2B). Since many of the GO terms overlap, we simplified the enrichment analysis to focus on general UniProt keywords (Figure 4A). Interestingly, we observed a notable enrichment of proteins with the keyword "glycolysis" (enrichment factor 3.08, corrected p value = 0.002). We investigated this further by filtering the rest, exercise, and recovery data for proteins involved in glycolysis (Figure 4B). Several of these glycolytic enzymes appeared in circulation with the present exercise protocol. Furthermore, analysis of the amino acid sequence of each protein (Petersen et al., 2011) revealed none of these proteins have a predicted signal sequence peptide suggestive of a classically secreted protein (Table S2A). Conversely, all proteins are annotated in the Vesiclepedia database (Kalra et al., 2012). These data suggest that cells secrete glycolytic enzymes in EVs during the high energy demands of exercise and support published works demonstrating that glycolytic enzymes delivered by small vesicles can influence glycolytic rate in recipient cells (Garcia et al., 2016; Zhao et al., 2016). While the functional relevance of this, from a metabolic standpoint, remains unclear, these findings support the view that proteins capable of changing biological function in recipient cells are secreted in EVs during incremental exercise, independently of classic protein secretion.

Exercise-Liberated EVs Demonstrate Tropism to the Liver

Fundamental to the hypothesis that EVs participate in tissue crosstalk during exercise is the uptake of these vesicles in recipient tissues. Indeed, that we observed little changes in vesicle protein abundance after 4 hr of recovery implies that the vesicle-cargoed proteins are removed from circulation via uptake into tissues. To investigate the biodistribution of EVs once they are liberated into circulation during exercise, we isolated EVs from treadmill-exercised or sedentary C57BL6/J donor mice and labeled them with lipophilic carbocyanine $DiOC_{18}(7)$ (DiR). These labeled EVs were then intravenously administered to recipient mice, which were then analyzed by whole-body intravital imaging. Three hours after injection of a 48-μg dose of labeled vesicles, we detected fluorescence in mice receiving vesicles from exercising, but not resting, donors (Figure 5A), indicating that vesicles liberated into circulation by exercise more readily concentrate in tissues in the abdominal viscera. We then carried out repeat experiments in mice receiving labeled vesicles from a single donor at a one-to-one ratio and observed fluorescent signal only in the liver (Figure S4A). Importantly, we discovered a significant difference in fluorescence in the livers of mice receiving vesicles from exercised versus rested donors 1 hr after injection (Figure 5B), indicating that vesicles liberated into circulation during exercise more readily localize in the liver.

SILAC Pulse-Chase Experiments Reveal Extensive Internalization of Exosomal/Small-Vesicle Protein Cargo into Recipient Cells

Several lines of evidence using luciferase reporter cell lines (Montecalvo et al., 2012), lipophilic dyes (Tian et al., 2013), and accompanying flow cytometry and confocal microscopy techniques (Mulcahy et al., 2014) support the view that small vesicles (and their cargo) are internalized into recipient cells. To investigate further the penetration of exosomes and small vesicles into live liver cells, we treated alpha mouse liver (AML12) cells with 1,1-dioctadecyl-3,3,3,3-tetramethylindodicarbocyanine (DiD) fluorescently labeled exosomes isolated via ultracentrifugation from C2C12 myotubes. Confocal microscopy analysis (Figure S3) revealed that cells were labeled with punctate DiD containing structures on and in the cells. Some DiD was also present on the plasma membrane of cells, suggesting that small-vesicle/cell fusion may have occurred, mixing membranes and releasing contents to the cell. We then adopted a quantitative proteomic approach to investigate further the incorporation of small-vesicle and exosomal-derived proteins into liver cells, using plasma samples obtained from a tissue bank of fully labeled $^{13}C_6$-lysine SILAC mice. In this model, wild-type C57BL/6 mice are fed chow containing stable isotope or "heavy" labeled lysine, which is incorporated into the entire mouse proteome (Kruger et al., 2008). These mice, therefore, secrete heavy labeled protein, distinguishable by MS, within EVs. We hypothesized that isolation of exosomes and small vesicles from heavy labeled plasma sampled after treadmill exercise would enable pulse chasing to confirm uptake into cells (Figure 6A). Nanoparticle tracking analysis revealed isolation of vesicles within the range attributed to exosomes and small vesicles (~90 nm) (Figure S5A). To assess the degree of incorporation of heavy labeled, EV-cargoed protein into recipient cells, we treated AML12 hepatocytes with (1) vesicles isolated from heavy labeled exercise plasma, (2) the depleted plasma fraction from which the vesicles were isolated from, or (3) a control containing only PBS. After a 4-hr incubation, we removed the conditioned media and washed the cells. We then analyzed the cell lysates via nano-UHPLC-MS/MS, using the software Maxquant (Cox et al., 2009), to identify

Figure 3. Exercise Induces the Enrichment in Circulation of Proteins Associated with the Biogenesis and Function of Small Vesicles and Exosomes

(A) Label-free quantitative (LFQ) data from arterial-derived plasma EVs are presented as volcano plots revealing results of two-sample t tests (exercise versus rest) following permutation-based false discovery rate (FDR) correction. Proteins highlighted in blue are significantly differentially expressed in circulation with exercise versus rest. Proteins belonging to the indicated group are indicated in red (n = 11).

(B) Gene ontology cellular component (GOCC) enrichment analysis on proteins significantly altered during exercise. GO terms are presented as a word cloud with the size of the word indicating the enrichment factor (degree of over-representation in the data calculated from the intersect between total number of proteins observed with the annotation and the number of these differentially regulated by exercise), and the color indicating the FDR-corrected p value. MVB, multivesicular body.

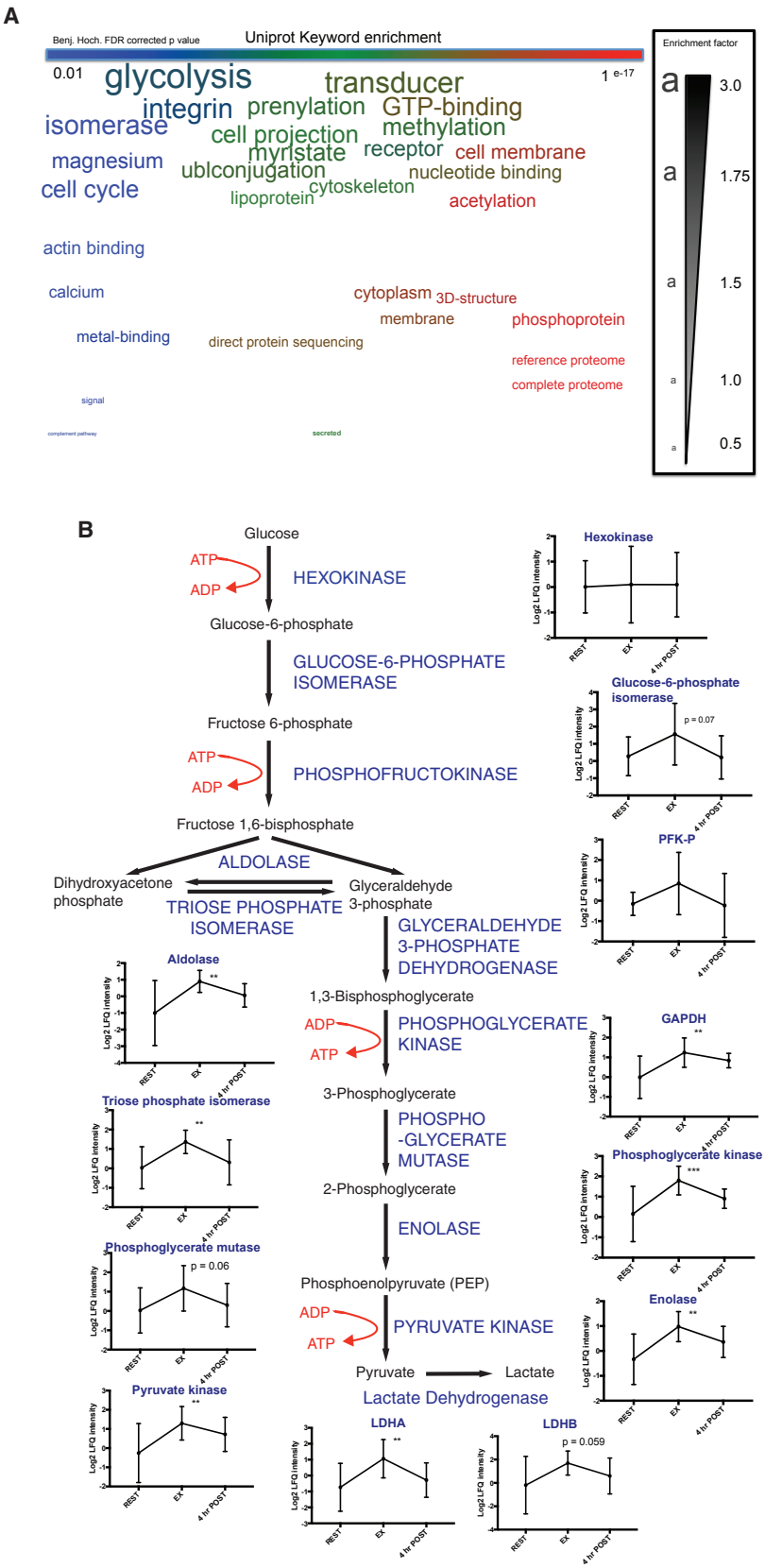

Figure 4. Exercise Induces a Significant Increase in Proteins Associated with a Wide Range of Biological Processes Including Glycolysis

(A) Fisher's exact test of categorical annotation enrichment. Significantly different proteins (exercise versus rest, arterial data) were compared with the measured data to identify UniProt keyword annotations that were significantly over-represented. Data are shown as a word cloud, with size indicating the enrichment factor and color indicating the FDR-corrected p value. A value of <1 indicates a de-enrichment. All indicated annotations are significant.

(B) The glycolytic pathway depicted alongside LFQ data (mean ± SD) of respective glycolytic proteins from arterial EV lysates. n = 11, **p < 0.01, ***p < 0.001. EX, exercise.

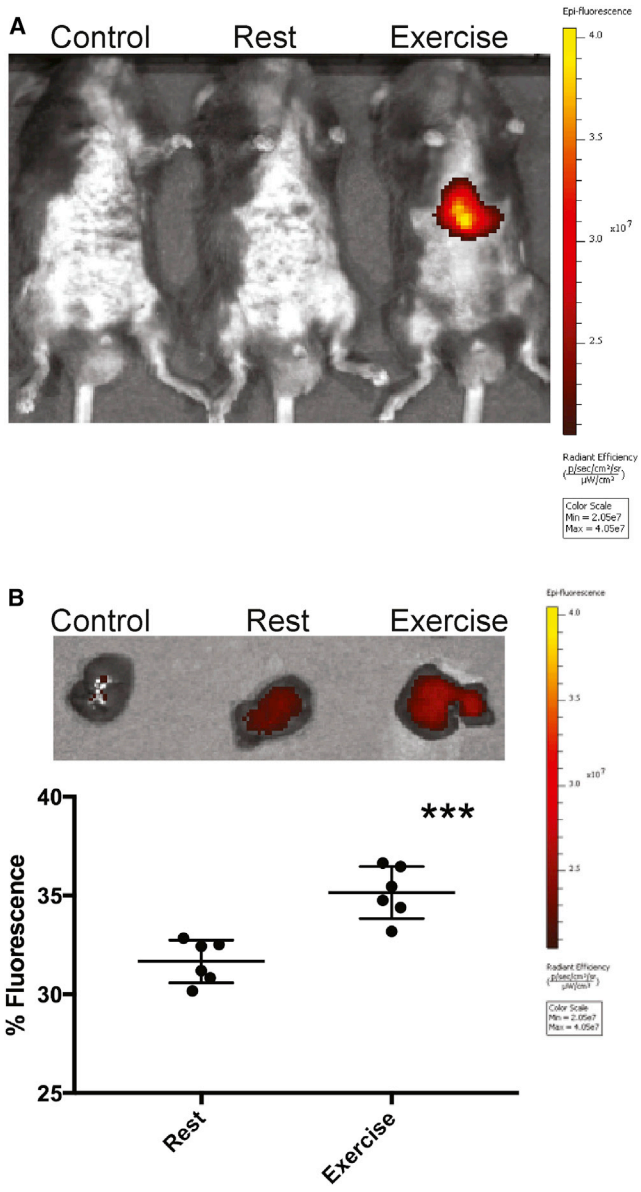

Figure 5. Intravital Imaging of Recipient Mice Treated Intravenously with DiR-Labeled Vesicles from Exercising or Rested Donor Mice

(A) Whole-body fluorescence imaging of animals treated with a 48-μg dose of vesicles from 12 exercised or sedentary donor mice. Images were taken 3 hr after tail vein injection. Max, maximum; Min, minimum.

(B) Quantitative fluorescent imaging of livers taken from recipient mice receiving a physiological (4 μg) dose of labeled vesicles from resting or exercised donors. Images were taken at 1 hr. Data are mean percentage fluorescence ± SD; ***$p < 0.001$; $n = 6$. Individual images are presented in Figure S4B.

proteins within the cell lysates that contained a heavy label (Figure 6A). In total we detected 6,531 proteins. As expected, treating cells with only PBS identified barely any heavy labeled proteins (<10 heavy labeled proteins potentially arising from false-positives [<0.24%]). The proteomic analysis of cells treated with heavy labeled plasma depleted of EVs identified proteins incorporated into the AML12 cells, largely associated with secreted peptides, glycoproteins, and regulators of immune and coagulation processes typical with circulating plasma proteins (Figure S5B). Importantly, parallel analyses of cells treated with small EVs revealed a large incorporation of the heavy labeled proteins, indicating transfer of vesicle-derived proteins. Furthermore, of the incorporated proteins identified, several markers of small vesicles (Figure 6B) and exosomes were present and heavy labeled, implying that not only were these proteins in circulating vesicles of exercised mice, but they were also transferred to recipient cells. These data support the notion that small vesicles and exosomes released from exercised mice can transfer their protein cargo to recipient cells. Indeed, by way of added support for this, we cross-referenced proteins elevated in circulation with exercise in our human dataset with their mouse homologues that were incorporated into hepatocytes from vesicle origins. GO cellular component enrichment analyses on this subset revealed they were of largely vesicular, endosomal, plasma membrane, and cell projection origins, indicating that exercise stimulates an increase in circulation of both exosomes and small vesicles and that these vesicles have the capacity to transfer their contents to live liver cells (Figure 6D). Also, we observed hepatocyte incorporation of vesicle-derived adhesion proteins such as tetraspanins and integrins thought to at least partially mediate vesicle-recipient cell interaction (Mulcahy et al., 2014) (Figure 6C).

Extracellular Vesicles Provide a Novel Mechanism for Myokine Secretion

While exercise has been shown to result in the release of biologically active molecules from many tissues, it is not surprising that the majority of exercise-induced secreted molecules originate from skeletal muscle, given that this is the organ undergoing contraction and major disruption to metabolic homeostasis. Since the initial discovery of IL6 as a myokine (Febbraio et al., 2004), several other myokine candidates have been proposed to mediate diverse biological functions, such as adipose tissue browning (Boström et al., 2012; Rao et al., 2014), cognition (Moon et al., 2016), and immune cell mobilization (Pedersen et al., 2016). Since our data show that exercise induces an efflux of EVs into the circulation, we postulated that this might be a mechanism by which skeletal muscle can release myokines independent of the classic secretory pathway. In an attempt to identify novel myokine candidates, we carried out a temporal quantitative proteomic analysis on EV fractions taken from indwelling catheters in the femoral vein of our 11 exercising human participants. By subtracting the quantitative assessments of proteins in these samples from those made in the previously described arterial sample analyses, and then factoring in the estimation of blood flow, we derived the net flux, either uptake or release, of over 600 proteins. In order to ensure high-confidence protein identifications and quantification we filtered the data on conservative criteria and vesicle annotation and observed 35 proteins with significant rates of release either during exercise or after recovery (Table 1). By way of preliminary validation of these myokine candidates, the majority of these proteins are expressed in skeletal muscle (Deshmukh et al., 2015), and Destrin, eukaryotic initiation factor 4A1, Tetraspanin CD151, and Integrin beta 5 (ITGB5) have been detected in EVs collected

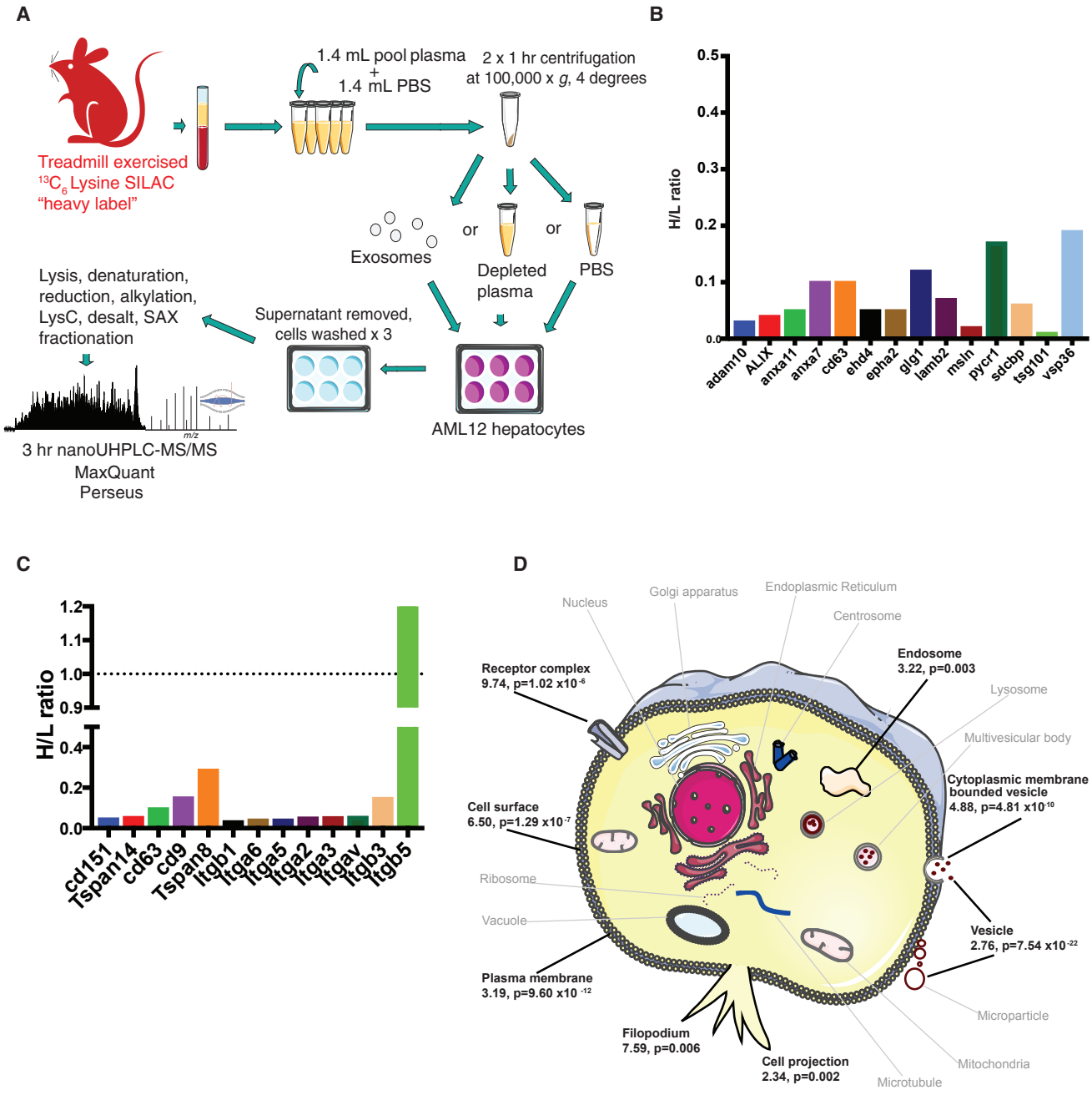

Figure 6. SILAC Pulse-Chase Experiment to Determine the Incorporation of EV-Cargoed Proteins into Hepatocytes

(A) Exosomes were isolated from plasma from fully labeled $^{13}C_6$ lysine SILAC mice via ultracentrifugation. The vesicles, plasma depleted of vesicles, or PBS (control) were then placed on AML12 hepatocytes for 4 hr, removed, and the cell lysates analyzed by nano-UHPLC-MS/MS.

(B and C) Heavy/light (H/L) metabolic label ratio of selected small-vesicle markers (B) and adhesion molecules (C) identified in hepatocyte lysates treated with vesicles derived from exercised Lys6 SILAC mice.

(D) Visual depiction of the cellular origin of proteins both enriched in circulation during exercise and transferred to hepatocytes from EVs isolated from exercised rodent plasma. Enrichment factor and FDR-corrected p value are indicated in bold. SAX, strong anion exchange.

from conditioned media of myotubes (Forterre et al., 2014). Consistent with our other EV datasets, 15 proteins with significant rates of release from the exercising limb do not have a predicted signal sequence peptide (Table S2B) (Petersen et al., 2011). Although validation of endocrine or paracrine function of these myokine candidates is warranted, these data provide evidence that EVs provide a novel mechanism in which myokines could be secreted. Of note, a wide array of cell types in different tissues and in circulation, such as immune cells and platelets, are known to release EVs. Aside from this estimation of the contribution of muscle-derived vesicles to the observed systemic effect, other cells may

Table 1. EV Trafficking as a Means for Myokine Secretion

Protein	Gene	Molecular Weight (kDa)	Rest log2 Net Flux (Mean ± SEM)	Exercise log2 Net Flux (Mean ± SEM)	Recovery log2 Net Flux (Mean ± SEM)	One-Sample t Test Significant: Rest	One-Sample t Test Significant: Exercise	One-Sample t Test Significant: Recovery	Two-Sample t Tests Significant: Rest versus Exercise	Two-Sample t Tests Significant: Rest versus Recovery	Vesiclepedia	Exocarta	Skeletal Muscle (Deshmukh et al., 2015)	Myotube EV (Forterre et al., 2014)	Signal Peptide
Alpha-1-antichymotrypsin	*SERPI NA3*	48	0.10 ± 0.22	−0.33 ± 0.18	−0.25 ± 0.20		✓				✓	✓			✓
Alpha-1-antitrypsin	*SERPI NA1*	47	0.62 ± 0.33	0.04 ± 0.34	−0.40 ± 0.20			✓		✓	✓	✓			✓
Alpha-2-antiplasmin	*SERPI NF2*	55	0.19 ± 0.19	−0.24 ± 0.10	−0.07 ± 0.15		✓		✓		✓	✓	✓		✓
Alpha-adducin	*ADD1*	70	0.22 ± 0.81	0.55 ± 0.59	−1.90 ± 0.60			✓			✓	✓	✓		
Apolipoprotein A-II	*APOA 2*	15	0.3 ± 0.19	−0.29 ± 0.22	0.41 ± 0.14			✓	✓		✓	✓	✓		✓
Basement membrane specific heparan sulfate proteoglycan core protein	*HSPG 2*	469	−1.30 ± 0.57	−0.62 ± 0.62	1.52 ± 0.51	✓		✓		✓	✓	✓	✓	✓	✓
Calcium and integrin binding protein	*CIB1*	22	0.41 ± 0.42	−0.12 ± 0.2	−0.26 ± 0.07			✓			✓	✓	✓		
Cathepsin D	*CTSD*	45	−0.43 ± 0.36	−0.51 ± 0.19	−1.32 ± 0.53		✓				✓	✓	✓		✓
Coagulation factor XIII B chain	*F13B*	76	−0.26 ± 0.40	−0.39 ± 0.15	0.60 ± 0.30		✓				✓		✓		✓
Corticosteroid-binding globulin	*SERPI NA6*	45	0.00 ± 0.27	−0.12 ± 0.35	−0.77 ± 0.30			✓			✓				✓
Cysteine-rich protein 2	*CRIP2*	21	0.55 ± 0.37	−0.23 ± 0.14	0.41 ± 0.63		✓				✓	✓	✓		
Destrin	*DSTN*	19	−0.08 ± 0.75	0.21 ± 0.44	−0.57 ± 0.11			✓			✓	✓	✓	✓	
Eukaryotic initiation factor 4A1	*EIF4A1*	46	−0.48 ± 0.33	0.44 ± 0.29	−0.86 ± 0.25			✓	✓		✓	✓	✓	✓	
Exostosin-like 2	*EXTL2*	37	−0.35 ± 0.37	−0.40 ± 0.18	−0.40 ± 0.21		✓				✓	✓	✓		
Extracellular matrix protein 1	*ECM1*	61	−0.42 ± 0.40	−0.32 ± 0.31	1.12 ± 0.29		✓		✓		✓		✓		✓
Fatty acid binding protein, adipocyte	*FABP4*	15	0.93 ± 0.43	−0.40 ± 0.21	0.02 ± 0.41		✓		✓		✓		✓		

(*Continued on next page*)

Table 1. ***Continued***

Protein	Gene	Molecular Weight (kDa)	Rest log2 Net Flux (Mean ± SEM)	Exercise log2 Net Flux (Mean ± SEM)	Recovery log2 Net Flux (Mean ± SEM)	One-Sample t Test Significant: Rest	One-Sample t Test Significant: Exercise	One-Sample t Test Significant: Recovery	Two-Sample t Tests Significant: Rest versus Exercise	Two-Sample t Tests Significant: Rest versus Recovery	Vesiclepedia	Exocarta	Skeletal Muscle (Deshmukh et al., 2015)	Myotube EV (Forterre et al., 2014)	Signal Peptide
Fibrinogen alpha chain	*FGA*	82	−0.14 ± 0.30	−0.12 ± 0.11	0.50 ± 0.16			✓			✓	✓			✓
Ficolin-3	*FCN3*	33	0.04 ± 0.24	−0.25 ± 0.11	0.09 ± 0.14		✓				✓	✓			✓
Glucose-6-phosphate 1-dehydrogenase	*G6PD*	49	0.73 ± 0.45	−1.23 ± 0.43	−0.98 ± 0.56		✓				✓	✓	✓		
Glucosidase 2 subunit beta	*PRKCSH*	60	0.15 ± 0.24	0.80 ± 0.40	−0.96 ± 0.38			✓			✓	✓	✓		✓
Human leukocyte antigen class II histocompatibility antigen, DR alpha chain	*HLA- DRA*	29	0.14 ± 0.44	−0.39 ± 0.17	0.38 ± 0.39		✓				✓	✓			✓
Hydrocephalus-inducing protein homologue	*HYDIN*	576	0.46 ± 0.31	0.19 ± 0.42	−0.64 ± 0.24			✓		✓	✓				
Integrin beta 5	*ITGB5*	88	0.62 ± 0.25	−0.47 ± 0.16	−0.16 ± 0.34		✓		✓		✓	✓	✓	✓	✓
Intercellular adhesion molecule 1	*ICAM1*	58	0.49 ± 0.17	−0.53 ± 0.24	−0.29 ± 0.24		✓		✓	✓	✓	✓	✓		✓
Mannan binding lectin serine protease 1	*MASP1*	79	−0.08 ± 0.17	−0.25 ± 0.15	0.30 ± 0.24		✓				✓	✓	✓		✓
MARKS-related protein	*MARKSL1*	20	1.21 ± 0.69	−0.05 ± 0.36	−1.05 ± 0.46			✓		✓	✓	✓	✓		
N-acetylmuramoyl-L-alanine amidase	*PGLYRP2*	62	0.59 ± 0.28	0.11 ± 0.35	−0.39 ± 0.19			✓		✓	✓	✓	✓		✓
Plasminogen	*PLG*	91	−0.19 ± 0.36	−0.08 ± 0.27	0.79 ± 0.25			✓			✓	✓	✓		✓
Protein FAM45A	*FAM45A*	40	0.15 ± 0.29	−0.53 ± 0.47	1.10 ± 0.32			✓			✓		✓		
Protein S100-A9	*S100A9*	13	0.49 ± 0.39	−0.27 ± 0.14	0.20 ± 0.20		✓				✓	✓	✓		
Ras-related protein Rab-1B	*RAB1B*	22	0.24 ± 0.94	−0.35 ± 0.71	−1.11 ± 0.38			✓			✓	✓	✓		
Serglycin	*SRGN*	18	−0.33 ± 0.47	−0.45 ± 0.22	−0.62 ± 0.55		✓				✓	✓	✓	✓	✓
Tetraspanin CD151	*CD151*	28	0.21 ± 0.34	−0.17 ± 0.34	−0.48 ± 0.19			✓		✓	✓	✓	✓	✓	

(*Continued on next page*)

CellPress

Table 1. *Continued*

Protein	Gene	Molecular Weight (kDa)	Rest log2 Net Flux (Mean ± SEM)	Exercise log2 Net Flux (Mean ± SEM)	Recovery log2 Net Flux (Mean ± SEM)	One-Sample t Test Significant: Rest	One-Sample t Test Significant: Exercise	One-Sample t Test Significant: Recovery	Two-Sample t Tests Significant: Rest versus Exercise	Two-Sample t Tests Significant: Rest versus Recovery	Vesiclepedia Exocarta	Skeletal Muscle (Deshmukh et al., 2015)	Myotube EV (Forterre et al., 2014)	Signal Peptide
Transmembrane channel-like protein 6	*TMC6*	90	−0.04 ± 0.60	−0.68 ± 0.19	−0.49 ± 0.51									
Vascular non-inflammatory molecule 2	*VNN2*	53	0.13 ± 0.36	−0.36 ± 0.17	−0.07 ± 0.51		✓			✓				✓

Mean net protein flux from the contracting limb before (Rest), immediately after (Exercise), and after 4 hr of recovery in 11 healthy male participants carrying out 1 hr (30 min at 55%, 20 min at 70%, and until exhaustion [~10 min] at 80% of VO_2max) of cycle exercise. Table details candidate myokines with significant rates of net release at exercise or post-recovery. Data are mean LFQ/mL/min/leg ± SEM and analyzed via one-sample t test to indicate significant difference from zero (no net uptake or release) at each time point. Also indicated are whether the protein had significantly different flux between pre- and post-exercise, pre- and post-recovery, vesicle (Vesiclepedia) or exosome (Exocarta) annotation, expression in skeletal muscle (Deshmukh et al., 2015), the EV fraction of myotube conditioned media (Forterre et al., 2014), or a predicted signal peptide sequence (SignalP 4.1).

also conceivably contribute to the pool of liberated vesicles during exercise, which warrants further investigation.

DISCUSSION

Exercise represents a highly complex perturbation of homeostasis in a large number of tissues, largely consequential of the increasing metabolic demands of contracting skeletal muscle. The integrated responses to these demands not only restore homeostasis in the short term, but also, when challenged regularly, produce adaptations associated with improved health and well-being (Hawley et al., 2014). While the concept of tissue crosstalk during exercise is, in itself, not novel, the field has focused upon uncovering new secretory factors that act in ligand-receptor binding complexes (Whitham and Febbraio, 2016). Here, we have utilized the enormous discovery potential of quantitative proteomics, in relatively simply derived samples, to reveal comprehensive and compelling evidence of a contribution of EV trafficking to the coordinated responses to exercise. Recognition that vast numbers of proteins that lack a signal sequence peptide can be secreted into circulation within EVs provides a paradigm shift in the concept of cell-cell communication during exercise.

Exosomes and small vesicles are heterogeneous nano-sized vesicles with unique protein, lipid, and nucleic acid compositions capable of eliciting different effects on recipient cells (Willms et al., 2016). That this heterogeneity might be coordinated during exercise is an intriguing concept. Elemental to this is the directed transport of vesicles to specific tissues. In support of this we herein show, at least in transplanted rodents, that the biodistribution of vesicles following a prolonged exercise bout differs from that seen in the absence of an exercise stimulus (Figure 5). Since blood flow in recipient animals would be equal, and the same amount of EVs from exercise and rest donors were injected, the observed difference in localization must be driven by factors intrinsic to the vesicles. The target specificity of small EVs is thought to be mediated by adhesion proteins such as integrins and tetraspanins on the surface of the vesicles (Raposo and Stoorvogel, 2013). Interestingly, we observed a significant increase in a wide range of adhesion proteins in the systemic circulation with exercise (Figure 3A) and many of these molecules were transferred to liver cells treated with EVs from exercised mice (Figure 6B). It is entirely conceivable, therefore, that localization of vesicles to specific tissues such as the liver is mediated by adhesion proteins found by us to be significantly different in circulation during exercise versus rest. Indeed, the liver-tropic metastatic behavior of selected tumor cells appears to correlate with ITGB5 expression in vesicles derived from these cells (Hoshino et al., 2015). Since we observed a significant release of ITGB5 from the exercising limb and a marked incorporation of this protein in liver cells treated with EVs from exercised mice (Figure 6B), it is tempting to speculate ITGB5 might be one adhesion protein involved in the complex systemic targeting of EVs to the liver during exercise.

The present data describing proteins circulating in EVs during exercise show non-random associations with a wide array of biological processes. While such enrichment analyses do not demonstrate causality, previous research supports the view that EVs are capable of mediating significant biological change

in recipient cells/tissues (Alexander et al., 2015; Thomou et al., 2017; Tkach and Théry, 2016; Ying et al., 2017). Allied to this, we show here, via femoral arteriovenous difference analysis, several novel myokine candidates released from the contracting limb via EVs, highlighting the potential for long-range signaling between tissues, independent of classic protein secretion and ligand/receptor binding complexes. As shown in Figure 4B, several enzymes in the glycolytic pathway were significantly increased in the exercise samples compared with the rest and recovery samples. Whether these glycolytic enzymes, or indeed other proteins, nucleic acids, and lipids packaged in EVs, play a role in modulating metabolism during exercise requires further study. Exercise exerts considerable metabolic demands on the human body and these are intuitively unequal among tissues. Since fundamental cellular processes like *de novo* protein translation and protein degradation cost energy (Kafri et al., 2016; Peth et al., 2013), vesicle trafficking of metabolic mediators might be an evolutionary conserved process by which tissues can share resources during the high energy demands of physical exertion. Although the temporal aspects of exosome and small-vesicle biogenesis and transport in an exercise context are unknown, the release of exosomes is generally associated with increases in intracellular calcium (Ca^{2+}) (Savina et al., 2003). Since motor neuron stimulation of skeletal muscle fibers leads to a rapid release of Ca^{2+} from the sarcoplasmic reticulum (Melzer et al., 1984), it is plausible that muscle has the capacity to release small vesicles rapidly into circulation and actuate signaling between important metabolic tissues.

We report here several candidate myokines that appear to be released into circulation in EVs during exercise. Notably, we observed little overlap between these newly identified proteins and those previously described in the literature, some of which have been identified in EVs (Safdar et al., 2016). However, our proteomic screen of the human samples was far from complete and we detail within our methods ways in which we can improve the observed quantitative coverage. Notably, this is possible in simply derived EV samples via high-speed centrifugation and proteomic sample preparation methods that are rapidly becoming routine.

In summary, we provide evidence for the involvement of EV trafficking in inter-tissue communication during exercise. The role of secreted proteins released from cells via classic secretory pathways to act as ligands for cell surface receptors during exercise is unequivocally important. Nonetheless, our data introduce a new paradigm, namely EV trafficking, by which tissue crosstalk during exercise can exert systemic biological effects.

STAR★METHODS

Detailed methods are provided in the online version of this paper and include the following:

- KEY RESOURCES TABLE
- CONTACT FOR REAGENT AND RESOURCE SHARING
- EXPERIMENTAL MODEL AND SUBJECT DETAILS
  - Human Participants
  - Animals
  - Cell Lines
- METHOD DETAILS
  - Exercise Study
  - Vesicle Isolation
  - Nanoparticle Tracking Analysis (NTA) & Cryo Electron Microscopy
  - Mass Spectrometry of EV Lysates
  - Intravital Imaging of Transpanted EVs
  - Confocal Imaging of Fluorescently Labelled Exosome Treated Cells
  - SILAC Pulse Chase *In Vitro* Experiment
- QUANTIFICATION AND STATISTICAL ANALYSIS
  - EV Exercise Data
  - IVIS Analysis
  - Silac Pulse Chase Data
- DATA AND SOFTWARE AVAILABILITY

SUPPLEMENTAL INFORMATION

Supplemental Information includes five figures and two tables and can be found with this article online at https://doi.org/10.1016/j.cmet.2017.12.001.

ACKNOWLEDGMENTS

The authors acknowledge Deb Ramsey and the team at Alfred Medical Research and Education Precinct Animal Services, Melbourne, Australia; Associate Professor Mark Molloy and staff of the Australian Proteomic Analysis Facility; and Dr. Martin Pal for assistance with the $^{13}C_6$-lysine mouse labeling. Furthermore, the authors would like to thank Prof. Tami Geiger and Dr. Michal Harel for advice on vesicle isolation and sample processing and Claire Vennin for assistance with the IVIS analysis, and also acknowledge the skilled assistance of Betina Bolmgren, Section of Molecular Physiology, Department of Nutrition, Exercise and Sports, University of Copenhagen, Denmark. We would also like to thank staff at the Garvan Institute of Medical Research, Clinical Research Facility and volunteers for assistance in providing plasma samples for method optimization and all volunteers for participating in the exercise experiments. This research has been facilitated by access to the University of Sydney's Mass Spectrometry Core Facility. This project was supported by grants from the Australian Research Council (DP130103573) and National Health and Medical Research Council (NHMRC) (APP1062436) to M.A.F. and M.W. M.A.F., B.J.P., and D.E.J. are Fellows of the NHMRC. The study was also funded by The Danish Research Council (DFF 1333-00029B/DFF00725B for M.F. and DFF 0602-02277B for J.F.P.W.) and The Novo Nordisk Foundation (R195-A16471 for J.F.P.W.), and M.F. was the recipient of a fellowship from the Danish Diabetes Academy funded by the Novo Nordisk Foundation.

AUTHOR CONTRIBUTIONS

Conceptualization, M.W., M.A.F., M.F., J.F.P.W., and E.A.R.; Methodology, M.W., B.L.P., B.K., K.I.W., P.G., J.F.P.W., and E.A.R.; Formal Analysis, M.W. and B.L.P.; Investigation, M.W., B.L.P., M.F., J.R.H., B.K., E.A.R., M.H., W.E.H., R.P.K., T.P., L.C., N.J., K.I.W., E.E., C.L.E., and J.F.P.W.; Resources, M.W., M.A.F., B.K., E.A.R., J.F.P.W., C.M.S., K.I.W., P.G., B.L.P., and D.E.J.; Writing – Original Draft, M.W., B.L.P., and M.A.F.; Writing – Review & Editing, all authors; Visualization, M.W., B.L.P., N.J., W.E.H., and R.P.K.; Supervision, M.W., M.A.F., B.K., J.F.P.W., E.A.R., D.E.J., and C.M.S.; Project Administration, M.W.; Funding Acquisition, M.A.F., M.W., M.F., J.F.P.W., and C.M.S.

Received: April 20, 2017
Revised: October 10, 2017
Accepted: November 30, 2017
Published: January 9, 2018

REFERENCES

Alexander, M., Hu, R., Runtsch, M.C., Kagele, D.A., Mosbruger, T.L., Tolmachova, T., Seabra, M.C., Round, J.L., Ward, D.M., and O'Connell,

R.M. (2015). Exosome-delivered microRNAs modulate the inflammatory response to endotoxin. Nat. Commun. *6*, 7321.

Booth, F.W., Roberts, C.K., and Laye, M.J. (2012). Lack of exercise is a major cause of chronic diseases. Compr. Physiol. *2*, 1143–1211.

Boström, P., Wu, J., Jedrychowski, M.P., Korde, A., Ye, L., Lo, J.C., Rasbach, K.A., Boström, E.A., Choi, J.H., Long, J.Z., et al. (2012). A PGC1-α-dependent myokine that drives brown-fat-like development of white fat and thermogenesis. Nature *481*, 463–468.

Cox, J., and Mann, M. (2008). MaxQuant enables high peptide identification rates, individualized p.p.b.-range mass accuracies and proteome-wide protein quantification. Nat. Biotechnol. *26*, 1367–1372.

Cox, J., Hein, M.Y., Luber, C.A., Paron, I., Nagaraj, N., and Mann, M. (2014). Accurate proteome-wide label-free quantification by delayed normalization and maximal peptide ratio extraction, termed MaxLFQ. Mol. Cell. Proteomics *13*, 2513–2526.

Cox, J., Matic, I., Hilger, M., Nagaraj, N., Selbach, M., Olsen, J.V., and Mann, M. (2009). A practical guide to the MaxQuant computational platform for SILAC-based quantitative proteomics. Nat. Protoc. *4*, 698–705.

Deshmukh, A.S., Murgia, M., Nagaraj, N., Treebak, J.T., Cox, J., and Mann, M. (2015). Deep proteomics of mouse skeletal muscle enables quantitation of protein isoforms, metabolic pathways, and transcription factors. Mol. Cell. Proteomics *14*, 841–853.

Egan, B., Hawley, J.A., and Zierath, J.R. (2016). SnapShot: exercise metabolism. Cell Metab. *24*, 342–342.e1.

Febbraio, M.A. (2017). Exercise metabolism in 2016: health benefits of exercise - more than meets the eye! Nat. Rev. Endocrinol. *13*, 72–74.

Febbraio, M.A., Hiscock, N., Sacchetti, M., Fischer, C.P., and Pedersen, B.K. (2004). Interleukin-6 is a novel factor mediating glucose homeostasis during skeletal muscle contraction. Diabetes *53*, 1643–1648.

Forterre, A., Jalabert, A., Berger, E., Baudet, M., Chikh, K., Errazuriz, E., De Larichaudy, J., Chanon, S., Weiss-Gayet, M., Hesse, A.M., et al. (2014). Proteomic analysis of C2C12 myoblast and myotube exosome-like vesicles: a new paradigm for myoblast-myotube cross talk? PLoS One *9*, e84153.

Frühbeis, C., Helmig, S., Tug, S., Simon, P., and Krämer-Albers, E.M. (2015). Physical exercise induces rapid release of small extracellular vesicles into the circulation. J. Extracell. Vesicles *4*, 28239.

Garcia, N.A., Moncayo-Arlandi, J., Sepulveda, P., and Diez-Juan, A. (2016). Cardiomyocyte exosomes regulate glycolytic flux in endothelium by direct transfer of GLUT transporters and glycolytic enzymes. Cardiovasc. Res. *109*, 397–408.

Geyer, P.E., Holdt, L.M., Teupser, D., and Mann, M. (2017). Revisiting biomarker discovery by plasma proteomics. Mol. Syst. Biol. *13*, 942.

Goldstein, M.S. (1961). Humoral nature of the hypoglycemic factor of muscular work. Diabetes *10*, 232–234.

Guescini, M., Canonico, B., Lucertini, F., Maggio, S., Annibalini, G., Barbieri, E., Luchetti, F., Papa, S., and Stocchi, V. (2015). Muscle releases alpha-sarcoglycan positive extracellular vesicles carrying miRNAs in the bloodstream. PLoS One *10*, e0125094.

Hansen, J., Brandt, C., Nielsen, A.R., Hojman, P., Whitham, M., Febbraio, M.A., Pedersen, B.K., and Plomgaard, P. (2011). Exercise induces a marked increase in plasma follistatin: evidence that follistatin is a contraction-induced hepatokine. Endocrinology *152*, 164–171.

Hansen, J.S., Clemmesen, J.O., Secher, N.H., Hoene, M., Drescher, A., Weigert, C., Pedersen, B.K., and Plomgaard, P. (2015). Glucagon-to-insulin ratio is pivotal for splanchnic regulation of FGF-21 in humans. Mol. Metab. *4*, 551–560.

Haraszti, R.A., Didiot, M.C., Sapp, E., Leszyk, J., Shaffer, S.A., Rockwell, H.E., Gao, F., Narain, N.R., DiFiglia, M., Kiebish, M.A., et al. (2016). High-resolution proteomic and lipidomic analysis of exosomes and microvesicles from different cell sources. J. Extracell. Vesicles *5*, 32570.

Harel, M., Oren-Giladi, P., Kaidar-Person, O., Shaked, Y., and Geiger, T. (2015). Proteomics of microparticles with SILAC Quantification (PROMIS-Quan): a novel proteomic method for plasma biomarker quantification. Mol. Cell. Proteomics *14*, 1127–1136.

Hawley, J.A., Hargreaves, M., Joyner, M.J., and Zierath, J.R. (2014). Integrative biology of exercise. Cell *159*, 738–749.

Hondares, E., Iglesias, R., Giralt, A., Gonzalez, F.J., Giralt, M., Mampel, T., and Villarroya, F. (2011). Thermogenic activation induces FGF21 expression and release in brown adipose tissue. J. Biol. Chem. *286*, 12983–12990.

Hoshino, A., Costa-Silva, B., Shen, T.-L.L., Rodrigues, G., Hashimoto, A., Tesic Mark, M., Molina, H., Kohsaka, S., Di Giannatale, A., Ceder, S., et al. (2015). Tumour exosome integrins determine organotropic metastasis. Nature *527*, 329–335.

Hurwitz, S.N., Rider, M.A., Bundy, J.L., Liu, X., Singh, R.K., and Meckes, D.G., Jr. (2016). Proteomic profiling of NCI-60 extracellular vesicles uncovers common protein cargo and cancer type-specific biomarkers. Oncotarget *7*, 86999–87015.

Jorfeldt, L., and Wahren, J. (1971). Leg blood flow during exercise in man. Clin. Sci. *41*, 459–473.

Kafri, M., Metzl-Raz, E., Jona, G., and Barkai, N. (2016). The cost of protein production. Cell Rep. *14*, 22–31.

Kalra, H., Simpson, R.J., Ji, H., Aikawa, E., Altevogt, P., Askenase, P., Bond, V.C., Borràs, F.E., Breakefield, X., Budnik, V., et al. (2012). Vesiclepedia: a compendium for extracellular vesicles with continuous community annotation. PLoS Biol. *10*, e1001450.

Kao, F.F., and Ray, L.H. (1954). Regulation of cardiac output in anesthetized dogs during induced muscular work. Am. J. Physiol. *179*, 255–260.

Keerthikumar, S., Chisanga, D., Ariyaratne, D., Al Saffar, H., Anand, S., Zhao, K., Samuel, M., Pathan, M., Jois, M., Chilamkurti, N., et al. (2015a). ExoCarta: a web-based compendium of exosomal cargo. J. Mol. Biol. *428*, 688–692.

Keerthikumar, S., Gangoda, L., Liem, M., Fonseka, P., Atukorala, I., Ozcitti, C., Mechler, A., Adda, C.G., Ang, C.-S.S., and Mathivanan, S. (2015b). Proteogenomic analysis reveals exosomes are more oncogenic than ectosomes. Oncotarget *6*, 15375–15396.

Korpelainen, R., Lämsä, J., Kaikkonen, K.M., Korpelainen, J., Laukkanen, J., Palatsi, I., Takala, T.E., Ikäheimo, T.M., and Hautala, A.J. (2016). Exercise capacity and mortality - a follow-up study of 3033 subjects referred to clinical exercise testing. Ann. Med. *48*, 1–8.

Kowal, J., Arras, G., Colombo, M., Jouve, M., Morath, J.P., Primdal-Bengtson, B., Dingli, F., Loew, D., Tkach, M., and Théry, C. (2016). Proteomic comparison defines novel markers to characterize heterogeneous populations of extracellular vesicle subtypes. Proc. Natl. Acad. Sci. USA *113*, E968–E977.

Kowal, J., Tkach, M., and Théry, C. (2014). Biogenesis and secretion of exosomes. Curr. Opin. Cell Biol. *29*, 116–125.

Kruger, M., Moser, M., Ussar, S., Thievessen, I., Luber, C.A., Forner, F., Schmidt, S., Zanivan, S., Fassler, R., and Mann, M. (2008). SILAC mouse for quantitative proteomics uncovers kindlin-3 as an essential factor for red blood cell function. Cell *134*, 353–364.

Lancaster, G.I., Møller, K., Nielsen, B., Secher, N.H., Febbraio, M.A., and Nybo, L. (2004). Exercise induces the release of heat shock protein 72 from the human brain in vivo. Cell Stress Chaperones *9*, 276–280.

Mann, M., Kulak, N.A., Nagaraj, N., and Cox, J. (2013). The coming age of complete, accurate, and ubiquitous proteomes. Mol. Cell *49*, 583–590.

Melzer, W., Rios, E., and Schneider, M.F. (1984). Time course of calcium release and removal in skeletal muscle fibers. Biophys. J. *45*, 637–641.

Mera, P., Laue, K., Ferron, M., Confavreux, C., Wei, J., Galán-Díez, M., Lacampagne, A., Mitchell, S.J., Mattison, J.A., Chen, Y., et al. (2016). Osteocalcin signaling in myofibers is necessary and sufficient for optimum adaptation to exercise. Cell Metab. *23*, 1078–1092.

Minciacchi, V.R., You, S., Spinelli, C., Morley, S., Zandian, M., Aspuria, P.-J.J., Cavallini, L., Ciardiello, C., Reis Sobreiro, M., Morello, M., et al. (2015). Large oncosomes contain distinct protein cargo and represent a separate functional class of tumor-derived extracellular vesicles. Oncotarget *6*, 11327–11341.

Montecalvo, A., Larregina, A.T., Shufesky, W.J., Stolz, D.B., Sullivan, M.L., Karlsson, J.M., Baty, C.J., Gibson, G.A., Erdos, G., Wang, Z., et al. (2012). Mechanism of transfer of functional microRNAs between mouse dendritic cells via exosomes. Blood *119*, 756–766.

Moon, H.Y., Becke, A., Berron, D., Becker, B., Sah, N., Benoni, G., Janke, E., Lubejko, S.T., Greig, N.H., Mattison, J.A., et al. (2016). Running-induced systemic cathepsin B secretion is associated with memory function. Cell Metab. *24*, 332–340.

Mulcahy, L., Pink, R., and Carter, D. (2014). Routes and mechanisms of extracellular vesicle uptake. J. Extracell. Vesicles *3*, https://doi.org/10.3402/jev.v3.24641.

Myers, J., Prakash, M., Froelicher, V., Do, D., Partington, S., and Atwood, J.E. (2002). Exercise capacity and mortality among men referred for exercise testing. N. Engl. J. Med. *346*, 793–801.

Pathan, M., Keerthikumar, S., Ang, C.-S.S., Gangoda, L., Quek, C.Y., Williamson, N.A., Mouradov, D., Sieber, O.M., Simpson, R.J., Salim, A., et al. (2015). FunRich: an open access standalone functional enrichment and interaction network analysis tool. Proteomics *15*, 2597–2601.

Pedersen, B.K., and Febbraio, M.A. (2012). Muscles, exercise and obesity: skeletal muscle as a secretory organ. Nat. Rev. Endocrinol. *8*, 457–465.

Pedersen, L., Idorn, M., Olofsson, G.H., Lauenborg, B., Nookaew, I., Hansen, R., Johannesen, H., Becker, J.C., Pedersen, K.S., Dethlefsen, C., et al. (2016). Voluntary running suppresses tumor growth through epinephrine- and IL-6-dependent NK cell mobilization and redistribution. Cell Metab. *23*, 554–562.

Petersen, T.N., Brunak, S., von Heijne, G., and Nielsen, H. (2011). SignalP 4.0: discriminating signal peptides from transmembrane regions. Nat. Methods *8*, 785–786.

Peth, A., Nathan, J.A., and Goldberg, A.L. (2013). The ATP costs and time required to degrade ubiquitinated proteins by the 26 S Proteasome. J. Biol. Chem. *288*, 29215–29222.

Pocsfalvi, G., Stanly, C., Vilasi, A., Fiume, I., Capasso, G., Turiák, L., Buzas, E.I., and Vékey, K. (2016). Mass spectrometry of extracellular vesicles. Mass Spectrom. Rev. *35*, 3–21.

Rao, R.R., Long, J.Z., White, J.P., Svensson, K.J., Lou, J., Lokurkar, I., Jedrychowski, M.P., Ruas, J.L., Wrann, C.D., Lo, J.C., et al. (2014). Meteorin-like is a hormone that regulates immune-adipose interactions to increase beige fat thermogenesis. Cell *157*, 1279–1291.

Raposo, G., and Stoorvogel, W. (2013). Extracellular vesicles: exosomes, microvesicles, and friends. J. Cell Biol. *200*, 373–383.

Rappsilber, J., Mann, M., and Ishihama, Y. (2007). Protocol for micro-purification, enrichment, pre-fractionation and storage of peptides for proteomics using StageTips. Nat. Protoc. *2*, 1896–1906.

Safdar, A., Saleem, A., and Tarnopolsky, M.A. (2016). The potential of endurance exercise-derived exosomes to treat metabolic diseases. Nat. Rev. Endocrinol. *12*, 504–517.

Savina, A., Furlán, M., Vidal, M., and Colombo, M.I. (2003). Exosome release is regulated by a calcium-dependent mechanism in K562 cells. J. Biol. Chem. *278*, 20083–20090.

Schindelin, J., Arganda-Carreras, I., Frise, E., Kaynig, V., Longair, M., Pietzsch, T., Preibisch, S., Rueden, C., Saalfeld, S., Schmid, B., et al. (2012). Fiji: an open-source platform for biological-image analysis. Nat. Methods *9*, 676–682.

Sjøberg, K.A., Holst, J.J., Rattigan, S., Richter, E.A., and Kiens, B. (2014). GLP-1 increases microvascular recruitment but not glucose uptake in human and rat skeletal muscle. Am. J. Physiol. Endocrinol. Metab. *306*, E355–E362.

Stanford, K.I., Middelbeek, R.J., Townsend, K.L., An, D., Nygaard, E.B., Hitchcox, K.M., Markan, K.R., Nakano, K., Hirshman, M.F., Tseng, Y.H., et al. (2013). Brown adipose tissue regulates glucose homeostasis and insulin sensitivity. J. Clin. Invest. *123*, 215–223.

Thomou, T., Mori, M.A., Dreyfuss, J.M., Konishi, M., Sakaguchi, M., Wolfrum, C., Rao, T.N., Winnay, J.N., Garcia-Martin, R., Grinspoon, S.K., et al. (2017). Adipose-derived circulating miRNAs regulate gene expression in other tissues. Nature *542*, 450–455.

Tian, T., Zhu, Y.L., Hu, F.H., Wang, Y.Y., Huang, N.P., and Xiao, Z.D. (2013). Dynamics of exosome internalization and trafficking. J. Cell. Physiol. *228*, 1487–1495.

Tkach, M., and Théry, C. (2016). Communication by extracellular vesicles: where we are and where we need to go. Cell *164*, 1226–1232.

Tyanova, S., Temu, T., Sinitcyn, P., Carlson, A., Hein, M.Y., Geiger, T., Mann, M., and Cox, J. (2016). The Perseus computational platform for comprehensive analysis of (prote)omics data. Nat. Methods *13*, 731–740.

Whitham, M., and Febbraio, M.A. (2016). The ever-expanding myokinome: discovery challenges and therapeutic implications. Nat. Rev. Drug Discov. *15*, 719–729.

Wiklander, O.P., Nordin, J.Z., O'Loughlin, A., Gustafsson, Y., Corso, G., Mäger, I., Vader, P., Lee, Y., Sork, H., Seow, Y., et al. (2015). Extracellular vesicle in vivo biodistribution is determined by cell source, route of administration and targeting. J. Extracell. Vesicles *4*, 26316.

Willms, E., Johansson, H.J., Mäger, I., Lee, Y., Blomberg, K.E., Sadik, M., Alaarg, A., Smith, C.I., Lehtiö, J., El Andaloussi, S., et al. (2016). Cells release subpopulations of exosomes with distinct molecular and biological properties. Sci. Rep. *6*, 22519.

Wojtaszewski, J.F., MacDonald, C., Nielsen, J.N., Hellsten, Y., Hardie, D.G., Kemp, B.E., Kiens, B., and Richter, E.A. (2003). Regulation of 5'AMP-activated protein kinase activity and substrate utilization in exercising human skeletal muscle. Am. J. Physiol. Endocrinol. Metab. *284*, E813–E822.

Ying, W., Riopel, M., Bandyopadhyay, G., Dong, Y., Birmingham, A., Seo, J., Ofrecio, J.M., Wollam, J., Hernandez-Carretero, A., Fu, W., et al. (2017). Adipose tissue macrophage-derived exosomal miRNAs can modulate in vivo and in vitro insulin sensitivity. Cell *171*, 372–384.

Zhao, H., Yang, L., Baddour, J., Achreja, A., Bernard, V., Moss, T., Marini, J.C., Tudawe, T., Seviour, E.G., San Lucas, F.A., et al. (2016). Tumor microenvironment derived exosomes pleiotropically modulate cancer cell metabolism. Elife *5*, e10250.

Zierath, J.R., and Wallberg-Henriksson, H. (2015). Looking ahead perspective: where will the future of exercise biology take us? Cell Metab. *22*, 25–30.

STAR★METHODS

KEY RESOURCES TABLE

REAGENT or RESOURCE	SOURCE	IDENTIFIER
Chemicals, Peptides, and Recombinant Proteins		
Sequencing grade modified trypsin	Promega	V5111
Lysyl Endopeptidase mass spectrometry grade	Wako	125-05061
Empore Anion-SR 47mm Extraction disks	Supelco Analytical	66888-U
Empore Styrene Divinyl Benzene (SDB-RPS) 47mm Extraction disks	Supelco Analytical	66886-U
Urea	Thermo Fisher Scientific	29700
Thiourea	Sigma	T7875
HEPES	Sigma	H3375
Trifluoroacetic acid LC-MS grade	Thermo Fisher Scientific	85183
LC-MS grade water	Thermo Fisher Scientific	51140
Qubit Protein Assay	Thermo Fisher Scientific	Q33211
Acetonitrile LC-MS grade	Thermo Fisher Scientific	51101
Formic Acid LC-MS grade	Thermo Fisher Scientific	85178
ReproSil-Pur 120 C18, 1.9 μm	Dr Maisch GmbH HPLC	R119.aq
DTT	Thermo Fisher Scientific	20291
IAA	Thermo Fisher	90034
Calcium Chloride	Sigma	C1016
Acetone	Sigma	650501
Acetic Acid	Sigma	320099
Phosphoric Acid	Sigma	466123
Boric Acid	Sigma	B6768
Sodium Hydroxide	Sigma	S8045
MouseExpress L-Lysine (13C,99%) Mouse Feed Kit	Cambridge isotopes	MLK-LYS-C
1,1-Dioctadecyl-3,3,3,3-tetramethylindodicarbocyanine (DiD) lipophilic dye	Life Technologies	V22887
$DiIC_{18}(7)$ "DiR" lipophilic dye	Life Technologies	D12731
Deposited Data		
Mass spectrometry proteomics data	This paper	The accession number for the mass spectrometry raw data reported in this paper is ProteomeXchange: PXD006501
Experimental Models: Cell Lines		
AML12 male mouse hepatocytes	ATCC	CRL-2254
C2C12 mouse myoblasts	ATCC	CRL-1772
Experimental Models: Organisms/Strains		
C57BL/6J mice	Jackson laboratories	000664
Software and Algorithms		
Maxquant v 1.5.5.1	Cox and Mann (2008)	http://www.biochem.mpg.de/5111795/maxquant
Perseus v 1.5.5.3	Tyanova et al. (2016)	http://www.biochem.mpg.de/5111795/maxquant
Funrich	Pathan et al. (2015)	http://www.funrich.org/
SignalP 4.1	Petersen et al. (2011)	http://www.cbs.dtu.dk/services/SignalP/
Living Image	Perkin Elmer	128113
Prism 7 for Mac	N/A	https://www.graphpad.com/scientific-software/prism/

CONTACT FOR REAGENT AND RESOURCE SHARING

Further information and requests for resources and reagents should be directed to and will be fulfilled by the Lead Contact, Mark Febbraio (m.febbraio@garvan.org.au).

EXPERIMENTAL MODEL AND SUBJECT DETAILS

Human Participants

One male and two female healthy volunteers donated 30 ml of whole blood after written informed consent for initial optimisation of methods. These procedures were approved by the St Vincents research ethics committee. For the human exercise study, twelve healthy males were recruited after written informed consent. One subject was excluded from the study due to poor sample condition and insufficient vesicle yield. General participant characteristics were as follows (Mean +/- SEM); Age 27 +/-1, body mass index 23.9 +/- 0.6 kg/m^2 , body fat 20.9 +/- 1.3%, fasting plasma glucose 98.9 +/- 1.8 mg/dL,. VO_2max 46.2 +/- 1.8 ml/kg/min. All procedures were approved by the regional ethics committee in Denmark (Journal number H-3-2012-140) and carried out in accordance with the Declaration of Helsinki II.

Animals

Eight week old, healthy male and female C57BL/6J mice were selected for SILAC labelling in order to create a tissue bank for spike-in or pulse-chase quantitative proteomics. Mice were paired for breeding in standard housing under standard light/dark cycle conditions while feeding ad libitum on custom $^{13}C_6$ Lysine chow (MouseExpress L-Lysine 13C6, 99%, Cambridge isotopes MLK-LYS-C). Resultant litters were weaned and paired again for F3 offspring, in order to allow full incorporation of the lysine label into the mouse proteome confirmed by mass spectrometry. For treadmill exercise eight week old male C57BL/6J were used and randomly assigned to treatment groups. All procedures were approved by the Alfred Medical Research Education Precinct and Garvan Institute/St Vincents Animal Ethics Committees, and animals were provided humane care in line with the ‘‘Principles of Laboratory Care’’ (NIH publication no. 85-23, revised 1985) and in accordance with the National Health and Medical Research Council of Australia Guidelines on Animal Experimentation.

Cell Lines

The immortalised, male mouse hepatocyte cell line AML12 was purchased from ATCC (CRL2254) and grown in a 1:1 mixture of Dulbecco’s modified Eagle’s medium (DMEM) and Ham’s F12 medium with 0.01 mg/ml insulin, 0.005 mg/ml transferrin, 6.7 ng/ml selenium, and 40 ng/ml dexamethasone, 90%; fetal bovine serum (FBS), 10%, in a humidified incubator at 37C, 5% CO_2. Media was changed 2 to 3 times a week. The immortalised, mouse skeletal muscle cell line C2C12 was purchased from ATCC (CRL-1772) and grown in DMEM supplemented with 10% FBS in a humidified incubator at 37C, 5% CO_2. Media was changed 2 to 3 times a week until 70% confluence after which cells were differentiated into myotubes in DMEM, 2% FBS.

METHOD DETAILS

Exercise Study

All participants were catheterized in the femoral artery and vein as previously described (Wojtaszewski et al., 2003) and subjected to bicycling at increasing intensities. Arterial and venous blood samples were taken at baseline and after 60 min of exercise (30 min at 55%, 20 min at 70% and until exhaustion (~10 min) at 80% of VO_2max) and after 4 hours of recovery. Blood was obtained in heparinised syringes and quickly transferred to microcentrifuge tubes and mixed with 30 μl 200mM EDTA /1500μl blood. Blood was rapidly (2 min) centrifuged at 15,000 g and plasma collected into clean microcentrifuge tubes. Samples were placed on ice until frozen at -80°C. Leg blood flow was measured using ultrasound techniques (a high-frequency 9-3 MHz linear array transducer in Power Doppler mode) during rest as previously described (Sjøberg et al., 2014) and estimated during exercise using the formula proposed by Jorfeldt and Wahren (1971)

Vesicle Isolation

For both human and rodent samples, plasma was defrosted on ice and centrifuged at 3,200g for 20min at 4°C to remove particulate matter. 1-6 ml pre-cleared plasma was then diluted in equal volumes of ice cold PBS and centrifuged for 60 min at 20,000g or 100,000g, 4°C. Supernatants were removed and the vesicle pellet was resuspended in ice cold PBS, followed by a repeat spin. Supernatants were removed and the vesicle pellets were lysed for mass spectrometry sample processing.

Nanoparticle Tracking Analysis (NTA) & Cryo Electron Microscopy

For both NTA and Cryo-EM, vesicle samples were resuspended in PBS. For NTA, EVs were measured and quantified using a Nanosight LM10-HS with a 532 nm laser running NTA v3.2 software. Immediately prior to measurement EV aggregates were broken up by gentle passage through a 29G needle. Samples were diluted empirically with 0.22μm filtered PBS to achieve 20 - 60 particles/frame (manufacturer’s optimum measurement range). Data were collected from 3 x 60 sec videos recorded at a constant 25°C with viscosity 1.05cP, camera level 9, detection threshold 5, and all other parameters set as default. For imaging, vitrified EV specimens were

analysed with cryo-TEM and were prepared using the following method; lacey carbon grids (Pro Sci Tech, QLD, Australia) were hydrophilized by glow discharge for 60 s (Pelco easiglow; Ted Pella, CA, USA). Specimens were then prepared within a controlled environment using the Leica EM GP (Leica, NSW, Australia), relative humidity 99% at 25°C. Two microliters of the sample solution was then pipetted onto the hydrophilized lacey grid, and blotted for 1.5s. The grid was then automatically plunged into liquid ethane at its freezing temperature (- 183°C) to form a vitrified layer. The grids were then transferred to a Dewar of liquid nitrogen (- 196°C) for transport and storage. The vitrified samples were examined using a FEI Tecani (FEI, OR, USA), operating at an accelerating voltage of 200kV. A Gatan 626 cryo holder (Gatan, CA, USA), was used to maintain the sample temperature below -172°C during both the transfer and imaging processes. Images were recorded digitally using an Eagle 2k CCD camera (FEI) and Digital Micrograph (Gatan). All samples were analysed using the low-dose software (FEI) to minimise beam exposure and electron beam radiation damage.

Mass Spectrometry of EV Lysates

Human EV pellets were lysed in denaturing lysis buffer containing 6M Urea, 2M Thiourea in 0.1M HEPES. Where source plasma volumes were greater than 1ml, lysates were precipitated in ice-cold acetone and resuspended in lysis buffer. Lysates were sonicated 2 x 30s in a Bioruptor, vortexed for 10 min and pulse spun before quantification by Qubit protein assay (Thermo Fisher Scientific). Samples were normalised for total protein and volume in lysis buffer before reduction in 10mM DTT for 1h, shaking at 800rpm. Samples were then alkylated in 25mM IAA, protected from light and shaken at 800rpm for 1h. Samples were quenched in the same volume of DTT followed by digestion in LysC (Wako) at a 1:20 ratio for 5h at room temperature. Samples were diluted in 5 volumes of 0.1M HEPES and further digested in trypsin (modified, Promega) overnight at 37°C at a ratio of 1:20 with 1mM CaCl added to aid digestion. Samples were acidified to a final concentration of 1% trifloroacetic acid and desalted on in-house made SDB-RPS (3M empore) stage tips as previously described (Rappsilber et al., 2007). Peptides were resuspended in loading buffer containing 2% acetonitrile, 0.5% acetic acid and loaded onto a 50cm x 75μm inner diameter column packed in house with 1.9μm C18AQ particles (Dr Maisch GmbH HPLC) using an Easy nLC-1000 UHPLC operated in single column mode loading at 700bar. Peptides were separated using a 180min linear gradient at a flow rate of 200nl/min using buffer A (0.1% formic acid) and a 5-30% buffer B (80% Acetonitrile, 0.1% formic acid). MS data were acquired on a Q Exactive classic operated in data dependent mode. MS spectra were acquired at 70,000 resolution, *m/z* range of 300-1750 and a target value of $3e^6$ ions, maximum injection time of 100ms. The top 20 precursor ions were isolated for MS/MS spectra after fragmentation with 2*m/z* isolation, $8.3e^5$ intensity threshold, normalised collision energy of 30 at 17,500 resolution at 200*m/z*, a 60ms injection time and $5e^5$ AGC target.

Intravital Imaging of Transpanted EVs

Donor C57BL/6J male mice were randomly assigned to either exercise or sedentary groups. Exercise mice were familiarised to treadmill running environment for 3-4 days prior to testing. Mice were exercised to exhaustion for ~90 min using a ramped treadmill exercise protocol starting at 10m/min and increasing by 2m/min every 10 min. Mice were defined as exhausted when remaining at the back of the treadmill for greater than 5 s despite gentle encouragement. Both exercised or sedentary mice were sedated by isoflurane inhalation and blood was sampled by cardiac puncture followed by euthanasia via cervical dislocation. Vesicle isolation was carried out as previously described and labelled in 1 μM DiR. 48μg or 4μg of washed, labelled vesicles from exercise or sedentary donors were injected via tail vein into male, 8 weeks old C57BL/6J recipients. Recipient animals and untreated controls were sedated by isoflurane inhalation and imaged at 1-3h post injection on an IVIS Spectrum (PerkinElmer). For tissue analysis, recipient mice were euthanized by cervical dislocation and tissues dissected and imaged. Fluorescence was detected using excitation and emission filters at 745nm and 800nm respectively.

Confocal Imaging of Fluorescently Labelled Exosome Treated Cells

AML12 cells were grown on glass coverslips (No.1.5) and were incubated for 4 hours with PBS with the lipophilic dye 1,1-Dioctadecyl-3,3,3,3-tetramethylindodicarbocyanine (DiD) or 18 μg protein equivalent of exosomes labelled with DiD. Cells were then fixed for 15 min. with 4% (w/v) paraformaldehyde in PBS and washed in PBS. Coverslips were stained with DAPI. Confocal images were generated on a Leica SP8 System with Hybrid GaAsP (HyD) detectors on a DMI 6000 stand equipped with 40x/1.10 (HCX PL APO W motCORR CS) and 63x/1.2 (HC PL APO W motCORR CS2) objectives, 405nm, 488nm (from ArKr laser), 561nm and 633nm excitation lasers running LAS X software (Leica, Wetzlar, Germany). Where required, image z stacks were obtained using the 'pinhole' set to 0.55 Airy units and oversampling more than 2x in x-y and z. Deconvolution was performed with Huygens Professional software (Scientific Volume Imaging, Hilversum, The Netherlands). Analysis was performed using LAS X and FiJi/ImageJ (Schindelin et al., 2012).

SILAC Pulse Chase *In Vitro* Experiment

$^{13}C_6$-Lysine labelled exosomes were isolated from plasma derived from a SILAC mouse tissue bank, as described above. Plasma was derived from 5 mice in total, with each mouse subjected to either a 30min or 90min treadmill exercise protocol or overnight fast prior to euthanasia and blood sampling. Isolated vesicles were pooled and resuspended in PBS. AML12 hepatocytes were gown to 80% confluence and changed to growth media with FBS replaced with EV depleted FBS (derived by overnight ultra-centrifugation at 100,000g). After 2 h, cells were spiked with 15 μg of SILAC vesicles or PBS control and incubated for 4 h. The supernatant was then removed and cells were washed x3 in ice cold PBS. Cells were lysed and scraped in 6M Urea, 2M Thiourea, 0.1M HEPES and transferred to a lo-bind microcentrifuge tube. Lysates were spun at 12,000rpm at 4°C for 20 min to remove cellular debris and sonicated 2 x 30 s on high in a bioruptor. Protein was precipitated by adding 1ml ice cold acetone, incubated overnight and spun at

2,000g for 15 min at 4°C. Pellets were dried and resuspended in lysis buffer by sonication. Samples were normalised for total protein and volume and were reduced and alkylated as described above. Protein digest was carried out by 2 x LysC (Wako) incubations (overnight and 8h) at a protease:protein ratio of 1:50. Peptides were acidified in 1% TFA and desalted as described above. Peptides were then fractionated by Strong Anion Exchange (SAX) using in-house stage tips packed with empore Anion exchange disks (3M). Peptides were eluted in BRUB buffer containing 20mM acetic acid, 20mM Phosphoric acid, 20mM boric acid altered to pH 11, 8, 6, 5, 4, and 2 with 1M Sodium Hydroxide. A seventh fraction was eluted in 10% TFA. All fractions were again desalted by SDB-RPS Stage tips and resuspended in loading buffer for nano-UHPLC MS/MS. Peptides were analysed using the same instrumentation and methods as indicated above for the EV lysates.

QUANTIFICATION AND STATISTICAL ANALYSIS

EV Exercise Data

Raw data files were searched against the human Uniprot database, downloaded on 27/09/16, using Maxquant v1.5.5.1. Data were analysed with variable (Oxidation (M), Acetyl (Protein N Term) and fixed (carbamidomethyl (C) modifications with label free quantitation and match between runs functions enabled. Protein quantitation was carried out on a minimum ratio count of 1 unique or razor peptide. Quantitative data were extracted from the protein groups files and analysed in Perseus (v 1.5.5.3). Proteins were mapped in Uniprot for their amino acid sequence and examined for signal peptide sequences using SignalP 4.1 (Petersen et al., 2011).

For all data sets, all proteins failing FDR but with a modified site, present in the decoy (reverse) database or known contaminants were filtered out prior to statistical analyses. For the arterial EV data, further filtering for a minimum of 3 values in each group was carried out, followed by normalisation of all data to a median of the resting values and $\log^2$ transformed. Exercise vs rest data were analysed via a paired, Two sample T test with an S0 of 0.1 and permutation based FDR correction $P<0.05$. Enrichment analyses were carried out by fishers exact test against significant proteins as a categorical annotation versus annotations derived from Uniprot and Vesiclepedia with Benjamini-Hochberg FDR truncation at a threshold value of 0.02. Presented in the manuscript are enrichment factors that indicate the degree of over-representation of a particular term calculated from the intersect between proteins observed with a particular term in the entire data set versus those changing with experimental intervention. Glycolytic protein data was filtered from the main data set and analysed individually via ANOVA to determine differences in protein expression at rest, exercise and recovery ($P<0.05$).

For A-V difference calculations, raw LFQ data from both arterial and venous samples were multiplied by corresponding haematocrit corrected blood flow data. Arterial data were then divided by venous data and filtered for a minimum of 4 values per condition, a minimum of 2 unique peptides and a minimum Andromeda score of 100. Data were then $\log^2$ transformed to derive net flux of protein around zero. Two sample T-tests were carried out to determine significant differences in protein flux between rest and exercise, along with 1 sample T-tests on exercise data to determine proteins presenting with a significantly different net protein flux from zero, $P<0.05$. Proteins of interest were mapped in Uniprot for their amino acid sequence and examined for signal peptide sequences using SignalP 4.1 (Petersen et al., 2011)

IVIS Analysis

Fluorescence data (total radiant efficiency) for each image was calculated using equal sized regions of interest in the Living Image software. Fluorescence was summed for all control, rest and liver images and each individual data point expressed as a percentage of total. Differences were determined via students T Test with significance set at $P<0.05$, calculated in the software package Prism.

Silac Pulse Chase Data

Raw data derived from hepatocyte fractions were searched against the mouse Uniprot database downloaded on 25/7/16 in Maxquant. Data were analysed with variable (Oxidation (M), Acetyl (Protein N Term) and fixed (carbamidomethyl (C) modifications with Lys6 labels and requantify, match between runs functions enabled. Peptide quantitation was carried out on a minimum of 2 peptide ratios. After removal of proteins failing FDR but with a modified site, present in the decoy (reverse) database or known contaminants, 1D annotation enrichment analysis was carried out on high values of H/L ratio, again versus GO terms from Uniprot.

DATA AND SOFTWARE AVAILABILITY

Searching of raw mass spec files and statistical analyses were carried out using Maxquant version 1.5.5.1 and Perseus v 1.5.5.3 available at http://www.biochem.mpg.de/5111795/maxquant. Gene mapping versus published datasets and creation of Venn diagrams to visualise comparative proteomic coverage were carried out in Funrich, available at http://www.funrich.org/. Signal peptide sequence analysis was carried out via SignalP 4.1 (http://www.cbs.dtu.dk/services/SignalP/) on amino acid sequences derived from Uniprot (http://www.uniprot.org/). The mass spectrometry proteomics data have been deposited to the ProteomeXchange Consortium via the PRIDE partner repository with the dataset identifier ProteomeXchange: PXD006501.

Cell Metabolism, Volume *27*

Supplemental Information

Extracellular Vesicles Provide a Means for Tissue Crosstalk during Exercise

Martin Whitham, Benjamin L. Parker, Martin Friedrichsen, Janne R. Hingst, Marit Hjorth, William E. Hughes, Casey L. Egan, Lena Cron, Kevin I. Watt, Rhiannon P. Kuchel, Navind Jayasooriah, Emma Estevez, Tim Petzold, Catherine M. Suter, Paul Gregorevic, Bente Kiens, Erik A. Richter, David E. James, Jørgen F.P. Wojtaszewski, and Mark A. Febbraio

Supplemental information

Figure S1. Related to STAR Methods. Deep proteomic analysis of EV proteome via nano-UHPLC MS/MS. (A) Log2 LFQ expression of proteins within samples isolated at 20,000g or 100,000g. Some common small vesicle and exosome markers are indicated. (B) Student's T Test of protein expression between samples derived at 20,000g or 100,000g with or without (C) FDR correction of P value.

Figure S2: Related to Figure 3. Gene ontology enrichment analysis of proteins upregulated by 1 h of cycle exercise in 11 human participants. (A) GOBP and GOMF (B) terms overrepresented in the significant data represented as a word cloud. Size of the word indicates the relative size of the enrichment factor whilst the colour indicates the Benjamini-Hochberg corrected P value. All terms indicated are significant ($P<0.02$).

Figure S3: Related to STAR methods. Confocal microscopy analysis of exosome internalisation into mouse liver hepatocytes. Representative confocal image of AML12 cells labelled with DiD (red) containing exosomes derived from C2C12 myotubes and DAPI (green) to identify nuclei (A). The DID label is present in punctate structures (B) and on the plasma membrane of the cell (C). Confocal sections of the cell showing corresponding orthogonal views confirming that many of the DiD labelled punctate structures are within the cell (D). Scale bars represent 10 µm

Figure S4: Related to Figure 5. Intravital Imaging analysis of mice receiving DiR labelled vesicles from rested or exercised donors. (A) Representative images of tissues taken 1h after injection of a physiological dose (4ug) of labelled vesicles. No signal was detected via whole body imaging (B) Raw images of each mice analysed in Figure 5B, (1h post injection, physiological dose N=6)

Figure S5: Related to Figure 6. SILAC pulse chase experiment to determine incorporation of EV proteins into AML12 hepatocytes. (A) NTA data indicating size of particles isolated by ultra-centrifugation and (B) 1D annotation enrichment analysis of proteins with the highest H/L ratio (incorporated proteins from labelled vesicles (B) or labelled, vesicle depleted plasma (C)). Each annotation is tested for protein H/L ratios that are systematically larger than the global distribution.

Data for each significant annotation are presented as Mean H/L ratio versus ranked FDR corrected P value (higher is more significant) and the number of significant proteins with that annotation are given in parentheses.

Table S2: Related to Figure 4, Table 1. Signal sequence prediction data for (A) Glycolytic proteins identified in EVs in the arterial circulation of 11 human participants carrying out 1h of cycle exercise and (B) for proteins with significant net release from the exercising limb. For each protein, the amino acid sequence is analysed for a distinguishable cleavage site and positions within signal peptides. Detailed are the maximal Cleavage (Cmax), Signal peptide (Smax) scores and their positions in the amino acid sequence, along with a combined cleavage score (Ymax) used to predict cleavage site. Smean provides the average S score of a possible signal peptide and D score is a weighted average of mean s and max Y scores, ultimately used to discriminate signal peptides. All non-secretory proteins score close to zero in all measures, with a default value of 0.450 used as a threshold for signal peptide identification

Supplementary Figure S1: Related to STAR methods

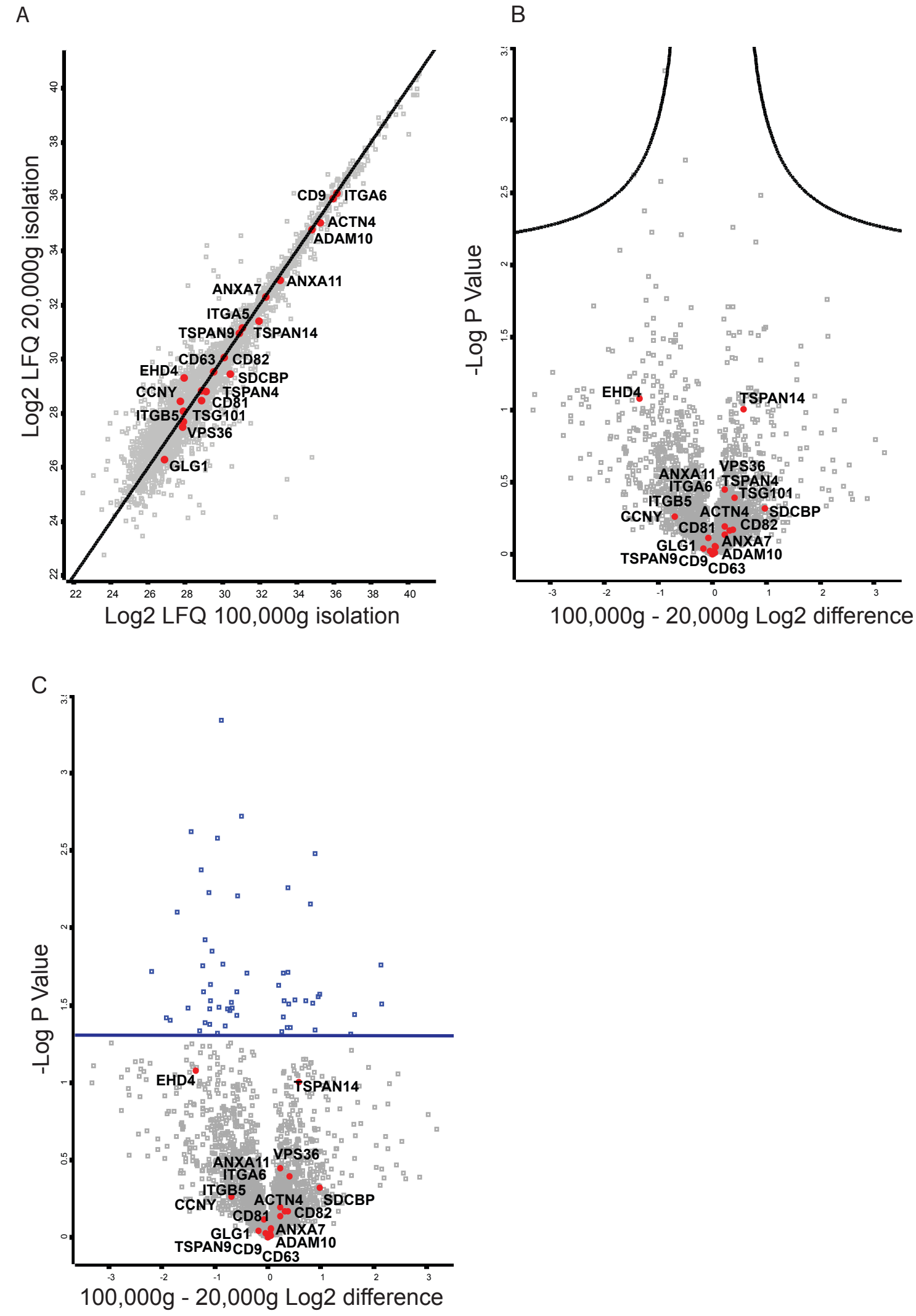

Supplementary Figure S2: Related to Figure 3

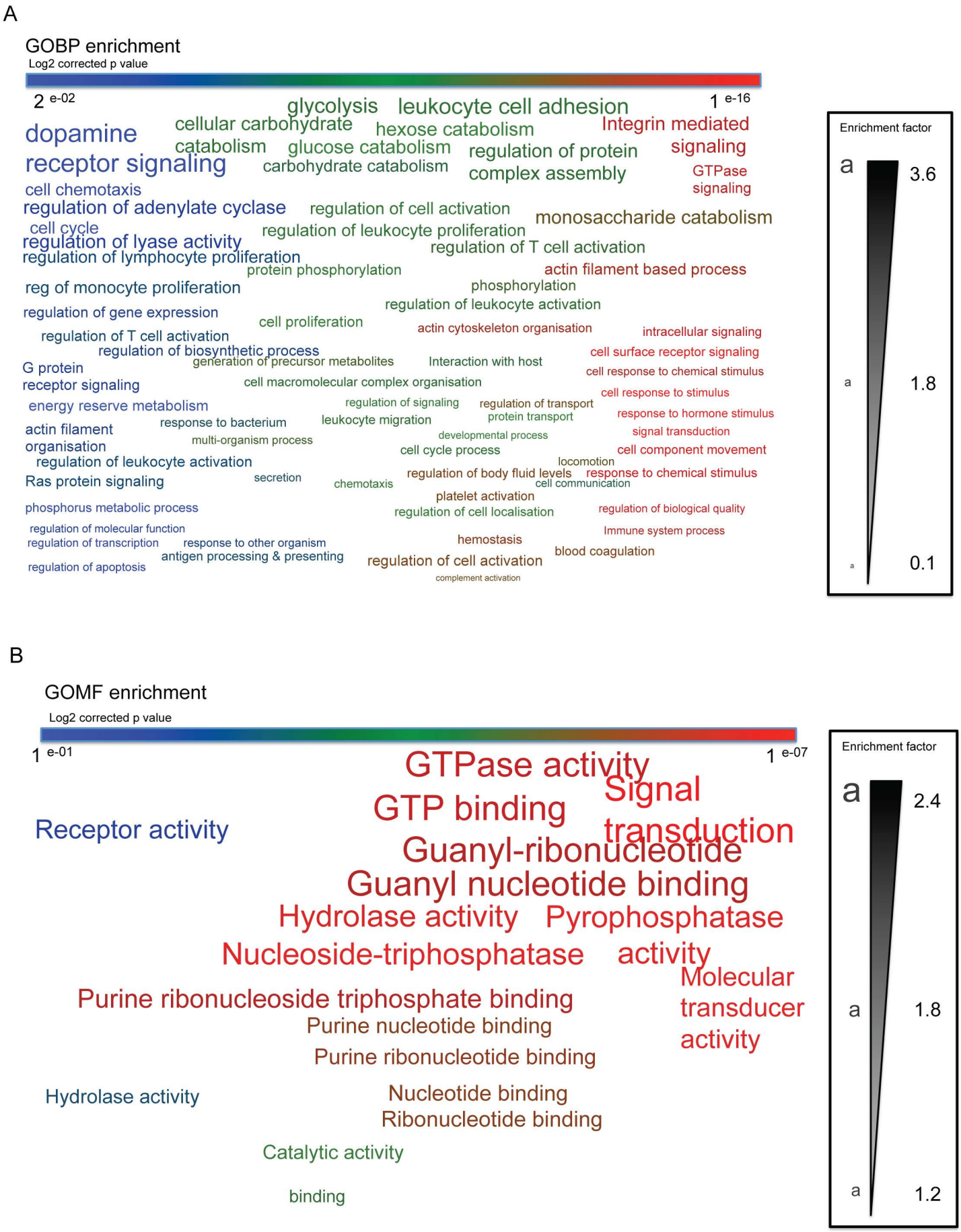

Supplementary Figure S3: Related to STAR methods

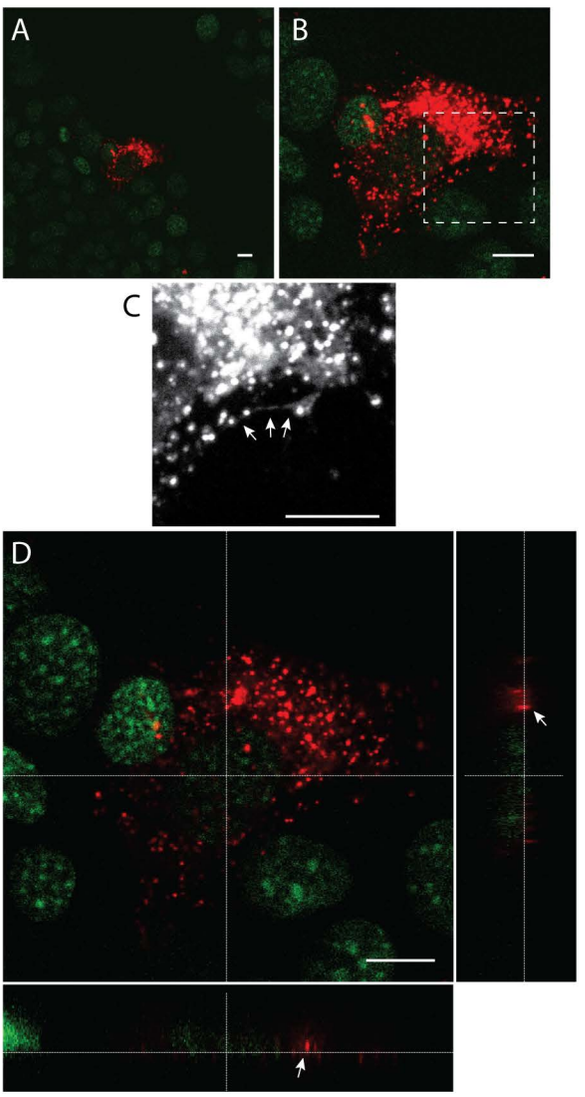

Supplementary Figure S4: Related to Figure 5

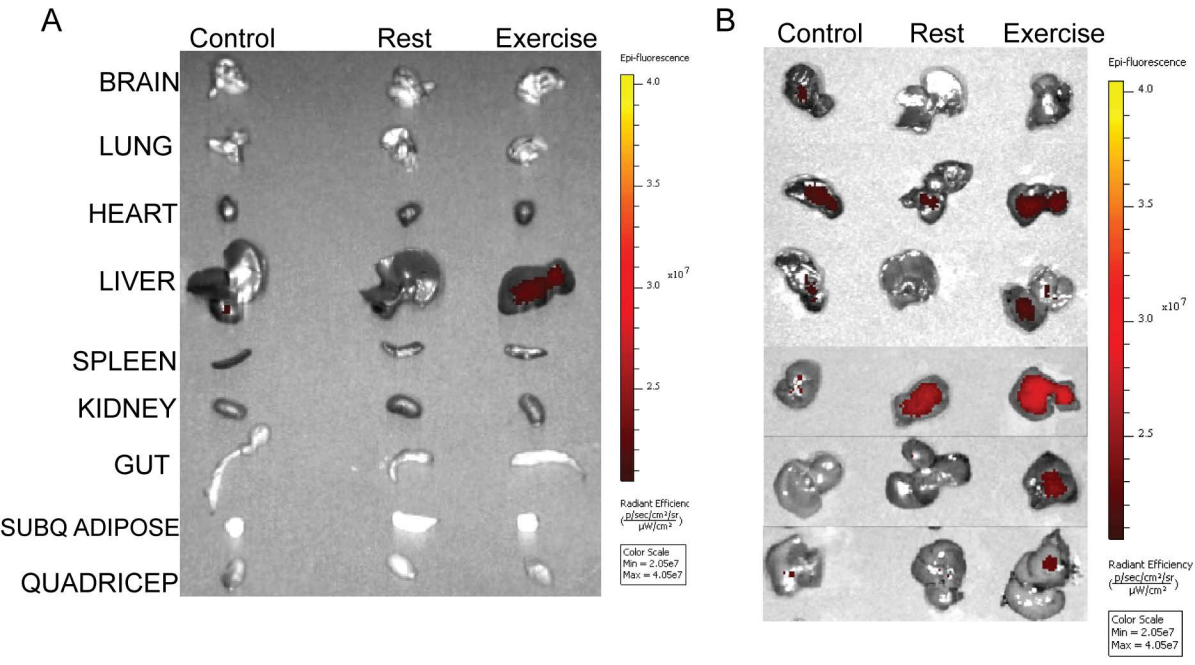

Supplementary Figure S5: Related to Figure 6.

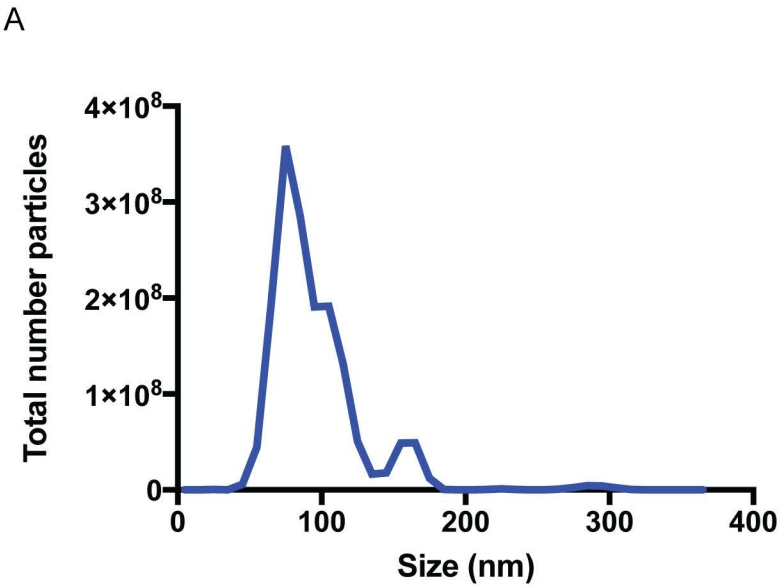

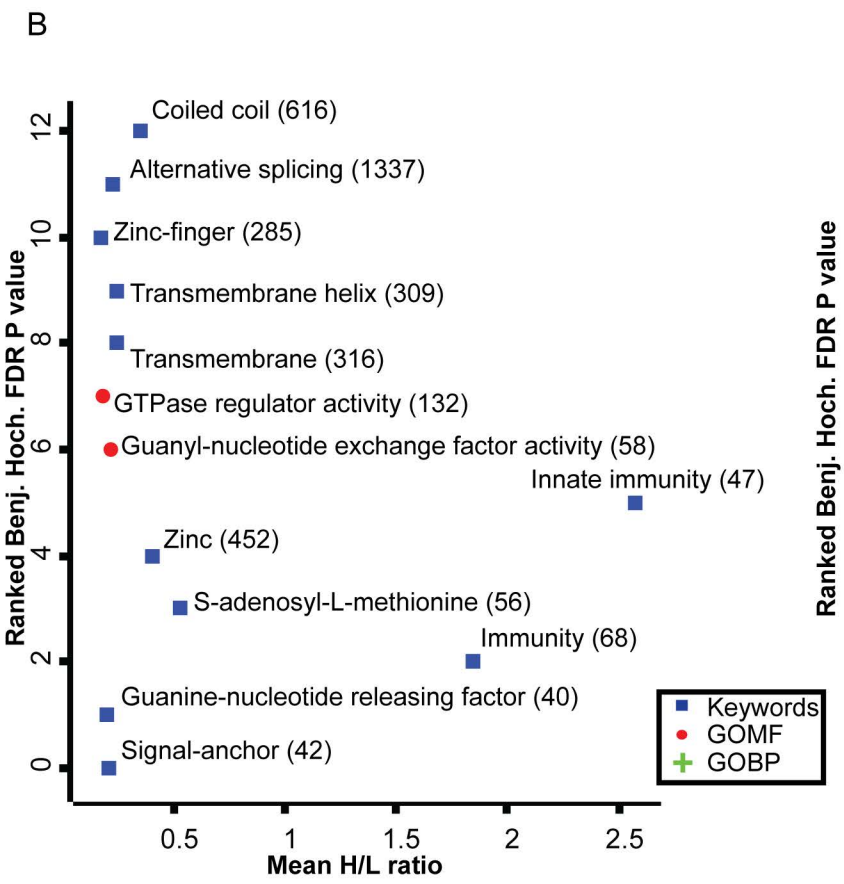

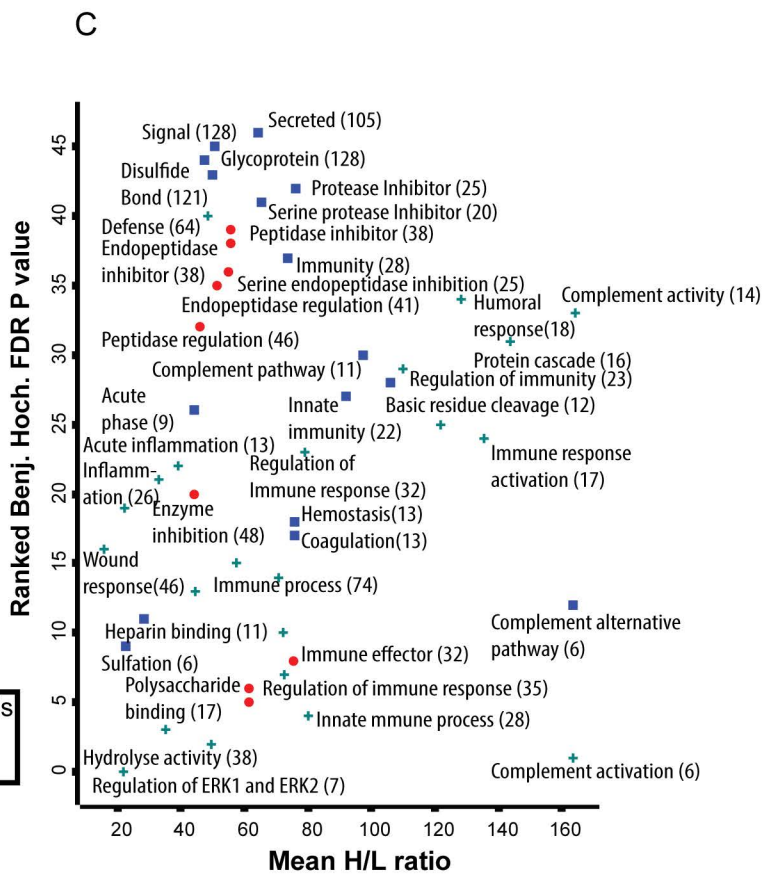

Table S2A: Related to Figure 4. Glycolytic proteins identified in EVs in arterial circulation during exercise

Protein	**Gene**	**Uniprot ID**	**Cmax**	**pos**	**Ymax**	**pos**	**Smax**	**pos**	**Smean**	**D**	**Signal peptide?**	**Dmaxcut**	**Networks-used**
Fructose-bisphosphate aldolase A	*ALDOA*	sp_P04075_ALDOA_HUMAN	0.108	65	0.104	65	0.108	60	0.097	0.100	No	0.450	SignalP-noTM
Alpha-enolase	*ENO1*	sp_P06733_ENOA_HUMAN	0.114	17	0.113	17	0.131	5	0.115	0.114	No	0.450	SignalP-noTM
Glyceraldehyde-3-phosphate dehydrogenase	*GAPDH*	sp_P04406_G3P_HUMAN	0.120	55	0.128	14	0.199	3	0.149	0.140	No	0.450	SignalP-noTM
Glucose-6-phosphate isomerase	*GPI*	sp_P06744_G6PI_HUMAN	0.110	32	0.106	29	0.117	21	0.101	0.103	No	0.450	SignalP-noTM
Hexokinase-1	*HK1*	sp_P19367_HXK1_HUMAN	0.109	17	0.123	12	0.179	5	0.136	0.130	No	0.450	SignalP-noTM
L-lactate dehydrogenase A chain	*LDHA*	sp_P00338_LDHA_HUMAN	0.123	37	0.106	46	0.124	32	0.090	0.100	No	0.500	SignalP-TM
L-lactate dehydrogenase B chain	*LDHB*	sp_P07195_LDHB_HUMAN	0.243	47	0.166	47	0.181	42	0.112	0.137	No	0.450	SignalP-noTM
ATP-dependent 6-phosphofructokinase, platelet type	*PFKP*	sp_Q01813_PFKAP_HUMAN	0.138	37	0.131	11	0.186	1	0.145	0.139	No	0.450	SignalP-noTM
Phosphoglycerate mutase 1	*PGAM1*	sp_P18669_PGAM1_HUMAN	0.114	15	0.120	15	0.225	14	0.132	0.126	No	0.450	SignalP-noTM
Phosphoglycerate kinase 1	*PGK1*	sp_P00558_PGK1_HUMAN	0.108	54	0.102	42	0.107	36	0.095	0.099	No	0.450	SignalP-noTM
Pyruvate kinase	*PKM*	sp_P14618_KPYM_HUMAN	0.248	24	0.176	24	0.160	7	0.125	0.148	No	0.450	SignalP-noTM
Triosephosphate isomerase	*TPI1*	sp_P60174_TPIS_HUMAN	0.287	27	0.179	27	0.170	25	0.112	0.143	No	0.450	SignalP-noTM

Table S2B. Related to Table 1: Signal peptide sequence analysis of proteins demonstrating significant net release from the exercising limb

Protein	Gene	Uniprot ID	Cmax	Pos	Ymax	Pos	Smax	Pos	Smean	D	Signal peptide?	Dmaxcut	Networks used
Alpha-adducin	*ADD1*	sp_P35611_ADDA_HUMAN	0.112	20	0.109	41	0.122	21	0.100	0.105	No	0.450	SignalP-noTM
Apolipoprotein A-II	*APOA2*	sp_P02652_APOA2_HUMAN	0.500	19	0.682	19	0.961	1	0.925	0.813	Yes	0.450	SignalP-noTM
Tetraspanin CD151	*CD151*	sp_P48509_CD151_HUMAN	0.135	44	0.131	12	0.203	11	0.175	0.149	No	0.500	SignalP-TM
Complement factor H	*CFH*	sp_P08603_CFAH_HUMAN	0.804	19	0.873	19	0.971	2	0.944	0.911	Yes	0.450	SignalP-noTM
Complement factor H-related protein 2	*CFHR2*	sp_P36980_FHR2_HUMAN	0.782	19	0.821	19	0.913	1	0.851	0.837	Yes	0.450	SignalP-noTM
Calcium and integrin-binding protein 1	*CIB1*	sp_Q99828_CIB1_HUMAN	0.116	31	0.114	11	0.186	2	0.120	0.117	No	0.450	SignalP-noTM
Cysteine-rich protein 2	*CRIP2*	sp_P52943_CRIP2_HUMAN	0.116	46	0.109	13	0.133	1	0.098	0.103	No	0.450	SignalP-noTM
Cathepsin D	*CTSD*	sp_P07339_CATD_HUMAN	0.573	21	0.700	21	0.926	5	0.850	0.781	Yes	0.450	SignalP-noTM
Destrin	*DSTN*	sp_P60981_DEST_HUMAN	0.107	61	0.106	37	0.122	22	0.099	0.102	No	0.450	SignalP-noTM
Extracellular matrix protein 1	*ECM1*	sp_Q16610_ECM1_HUMAN	0.488	20	0.632	20	0.874	11	0.820	0.734	Yes	0.450	SignalP-noTM
Eukaryotic initiation factor 4A-I	*EIF4A1*	sp_P60842_IF4A1_HUMAN	0.112	34	0.106	34	0.123	3	0.101	0.103	No	0.450	SignalP-noTM
Exostosin-like 2;Processed exostosin-like 2	*EXTL2*	sp_Q9UBQ6_EXTL2_HUMAN	0.407	38	0.290	38	0.428	34	0.237	0.268	No	0.500	SignalP-TM
Coagulation factor XIII B chain	*F13B*	sp_P05160_F13B_HUMAN	0.601	21	0.704	21	0.905	15	0.828	0.771	Yes	0.450	SignalP-noTM
Fatty acid-binding protein, adipocyte	*FABP4*	sp_P15090_FABP4_HUMAN	0.159	15	0.127	15	0.115	47	0.101	0.113	No	0.450	SignalP-noTM
Protein FAM45A	*FAM45A*	sp_Q8TCE6_FA45A_HUMAN	0.190	25	0.156	25	0.179	16	0.128	0.141	No	0.450	SignalP-noTM
Ficolin-3	*FCN3*	sp_O75636_FCN3_HUMAN	0.342	24	0.548	24	0.985	11	0.880	0.727	Yes	0.450	SignalP-noTM
Fibrinogen alpha chain;	*FGA*	sp_P02671_FIBA_HUMAN	0.579	20	0.721	20	0.940	1	0.890	0.812	Yes	0.450	SignalP-noTM
Glucose-6-phosphate 1-dehydrogenase	*G6PD*	sp_P11413_G6PD_HUMAN	0.127	42	0.118	11	0.155	44	0.116	0.117	No	0.450	SignalP-noTM
HLA class II histocompatibility antigen,	*HLA-DRA*	sp_P01903_DRA_HUMAN	0.641	26	0.701	26	0.896	5	0.772	0.739	Yes	0.450	SignalP-noTM

DR alpha chain													
Basement membrane-specific heparan sulfate proteoglycan core protein	*HSPG2*	sp_P98160_PGBM_HUMAN	0.610	22	0.766	22	0.982	8	0.963	0.873	Yes	0.450	SignalP-noTM
Hydrocephalus-inducing protein homolog	*HYDIN*	sp_Q4G0P3_HYDIN_HUMAN	0.120	27	0.125	11	0.169	4	0.136	0.131	No	0.450	SignalP-noTM
Intercellular adhesion molecule 1	*ICAM1*	sp_P05362_ICAM1_HUMAN	0.811	28	0.812	28	0.938	1	0.824	0.819	Yes	0.450	SignalP-noTM
Integrin beta-5	*ITGB5*	sp_P18084_ITB5_HUMAN	0.458	25	0.642	25	0.955	17	0.899	0.781	Yes	0.450	SignalP-noTM
MARCKS-related protein	*MARCKSL1*	sp_P49006_MRP_HUMAN	0.116	29	0.111	11	0.135	1	0.106	0.108	No	0.450	SignalP-noTM
Mannan-binding lectin serine protease 1	*MASP1*	sp_P48740_MASP1_HUMAN	0.868	20	0.829	20	0.879	13	0.790	0.808	Yes	0.450	SignalP-noTM
N-acetylmuramoyl-L-alanine amidase	*PGLYRP2*	sp_Q96PD5_PGRP2_HUMAN	0.758	22	0.842	22	0.973	12	0.935	0.893	Yes	0.450	SignalP-noTM
Plasminogen	*PLG*	sp_P00747_PLMN_HUMAN	0.801	20	0.773	20	0.854	16	0.762	0.767	Yes	0.450	SignalP-noTM
Glucosidase 2 subunit beta	*PRKCSH*	sp_P14314_GLU2B_HUMAN	0.579	15	0.728	15	0.945	7	0.908	0.825	Yes	0.450	SignalP-noTM
Ras-related protein Rab-1B	*RAB1B*	sp_Q9H0U4_RAB1B_HUMAN	0.160	35	0.141	35	0.197	17	0.130	0.135	No	0.450	SignalP-noTM
Protein S100-A9	*S100A9*	sp_P06702_S10A9_HUMAN	0.114	28	0.104	43	0.121	35	0.095	0.099	No	0.450	SignalP-noTM
Alpha-1-antitrypsin;Short peptide from AAT	*SERPINA1*	sp_P01009_A1AT_HUMAN	0.878	25	0.902	25	0.977	5	0.927	0.916	Yes	0.450	SignalP-noTM
Alpha-1-antichymotrypsin;Alpha-1-antichymotrypsin His-Pro-less	*SERPINA3*	sp_P01011_AACT_HUMAN	0.718	24	0.787	24	0.968	5	0.865	0.829	Yes	0.450	SignalP-noTM
Corticosteroid-binding globulin	*SERPINA6*	sp_P08185_CBG_HUMAN	0.606	23	0.714	23	0.947	3	0.841	0.783	Yes	0.450	SignalP-noTM
Alpha-2-antiplasmin	*SERPINF2*	sp_P08697_A2AP_HUMAN	0.432	28	0.531	28	0.982	1	0.713	0.630	Yes	0.450	SignalP-noTM
Serglycin	*SRGN*	sp_P10124_SRGN_HUMAN	0.869	28	0.890	28	0.973	16	0.914	0.903	Yes	0.450	SignalP-noTM
Transmembrane channel-like protein 6	*TMC6*	sp_Q7Z403_TMC6_HUMAN	0.147	17	0.141	17	0.173	5	0.140	0.141	No	0.450	SignalP-noTM
Vascular non-inflammatory molecule 2	*VNN2*	sp_O95498_VNN2_HUMAN	0.250	23	0.437	23	0.851	5	0.764	0.614	Yes	0.450	SignalP-noTM